Comparing 20 years of precipitation estimates from different sources over the world ocean

Karine Béranger, Bernard Barnier, Sergei K. Gulev, Michel Crépon

Comparing 20 years of precipitation estimates from different sources over the world ocean

Karine Béranger · Bernard Barnier · Sergei Gulev · Michel Crépon

Abstract The paper compares ten different global precipitation data sets over the oceans and discusses their respective strengths and weaknesses in ocean regions where they are potentially important to the salinity and buoyancy budgets of surface waters. Data sets (acronyms of which are given in Section 2) are categorised according to their source of data, which are (1) *in situ* for Center for Climatic Research (Legates and Willmott, 1990; Archive of Precipitation Version 3.01, http://climate.geog.udel.edu/~climate), Southampton Oceanography Centre (SOC) (Josey et al., *J Clim* 12:2856–2880, 1999) and University of Wisconsin-Milwaukee (UWM) (Da Silva et al. 1994); (2) *satellite* for Microwave Sounding Unit (MSU) (Spencer, *J Clim* 6:1301–1326, 1993), TOPEX (Quartly et al., *J Geophys Res* 104:31489–31516, 1999), and Hamburg Ocean Atmosphere Parameters and Fluxes from Satellite (HOAPS) (Bauer and Schluessel, *J Geophys Res* 98:20737–20759, 1993); (3) *atmospheric forecast model re-analyses* for European Centre for Medium-range Weather Forecast (ECMWF) (Gibson et al. 1997) and National Center for Environmental Prediction (NCEP) (Kalnay et al., *Bull Am Meteorol Soc* 77:437–471, 1996); and (4) *composite* for Global Precipitation Climatology Project (GPCP) (satellites and rain gauges, Huffman et al., *Bull Am Meteorol Soc* 78 (1):5–20, 1997) and Climate Prediction Center Merged Analysis of Precipitation (CMAP) (satellites, rain gauges and atmospheric forecast model, Xie and Arkin, *Bull Am Meteorol Soc* 78(11):2539–2558, 1997). Although there is no absolute field of reference, composite data sets are often considered as the best estimates. First, a qualitative comparison is carried out, which provides for each data set, a description of the geographical distribution of the climatological mean precipitation field. A more careful comparison between data sets is undertaken over periods they have in common. First, six among the ten data sets (SOC, UWM, ECMWF, NCEP, MSU and CMAP) are compared over their common period of 14 years, from 1980 to 1993. Then CMAP is compared to GPCP over the 1988–1995 period and to HOAPS over the 1992–1998 period. Usual diagnostics, like comparison of the precipitation patterns exhibited in the annual climatological means of zonal averages and global budget, are used to investigate differences between the various precipitation fields. In addition, precipitation rates are spatially integrated over 16 regional boxes, which are representative of the major ocean gyres or large-scale ocean circulation patterns. Seasonal and inter-annual variations are studied over these boxes in terms of time series anomalies or correlation coefficients. The analysis attempts to characterise differences and biases according to the original source of data (i.e. in situ or satellite, etc.). Qualitative agreement can be observed in all climatologies, which reproduce the major characteristics of the precipitation patterns over the oceans. However, great disagreements occur in terms of quantitative values and regional patterns, especially in regions of high precipitation. However, a better agreement is generally found in the northern hemisphere. The most significant differences, observed between data sets in the mean seasonal cycles and interannual variations, are discussed. A major result of the paper, which was not expected a priori, is that differences between data sets are much more dependent upon the ocean region that is considered than upon the origin of the data sets

K. Béranger (✉)
ENSTA, UME, Chemin de la Hunière,
91761 Palaiseau Cedex, France
e-mail: Karine.Beranger@ensta.fr
Tel.: +33-169319753
Fax: +33-169319997

B. Barnier
LEGI-IMG, CNRS UMR 5519, BP 53,
38041 Grenoble Cedex, France

S. Gulev
P. P. Shirshov Institute of Oceanology,
RAS, 36 Nakhimousky ave.
117851, Moscow, Russia

M. Crépon
LOCEAN,
Tour 45-55, 4e Etage, 4 Place Jussieu,
75252 Paris Cedex 05, France

(in situ vs satellite vs model, etc.). Our analysis did not provide enough objective elements, which would allow us to clearly recommend a given data set as reference or best estimate. However, composite data sets (GPCP, and especially CMAP), because they never appeared to be really "off" when compared to other data sets, may represent the best recent data set available. CMAP would certainly be our first choice to drive an ocean GCM.

Keywords Global ocean precipitation · Freshwater · Seasonal variability · Interannual variability

1 Introduction

The freshwater input in the ocean comes from precipitation, river runoff, sea ice and glacial melt. It can strongly increase the ocean vertical stability and exert a significant control on water mass transformation (Speer and Tziperman 1992). The increasing attention given to the distribution of sea surface salinity and its variations (Font et al. 2004) allowed the demonstration that, even in regions of strong advection, the behaviour of the sea surface salinity could not be dissociated from precipitation and evaporation rates (Delcroix et al. 1996). Thus, precipitation (*P* hereafter), which is a major component of the ocean freshwater input, is undeniably an essential contributor to the ocean buoyancy forcing, and its importance to ocean dynamics is fully recognised.

Nevertheless, most ocean General Circulation Models (OGCMs) used to study ocean processes and ocean variability are still using some relaxation to climatological values of the sea surface salinity in their freshwater forcing parameterisation (Large et al. 1997; Barnier 1998). A reason given is the great inaccuracy of mean *P* (and evaporation) estimates over the ocean, which must be compensated by some control on the sea surface salinity, although an inaccurate representation of the salinity seasonal cycle is often attributed to the relaxation itself (Killworth et al. 2000; Ferry and Reverdin 2004).

The need for suitable global *P* estimates over long time series has been brought out in an acute way by the societal concern to understand and predict climate changes in the atmosphere and in the ocean (Schmitt 1995) and by the application of OGCMs to a growing variety of problems. Frequent OGCM applications are made at very high resolution to investigate the driving mechanisms of the mean and variable ocean circulation (Smith et al. 2000; Willebrand et al. 2001; Tréguier et al. 2003). Interdisciplinary applications are emerging, investigating the natural variability of large marine ecosystems (Carmillet et al. 2001; Marchesiello et al. 2003), and ocean forecasting is developing rapidly (Ballabrera-Poy et al. 2002) with the management of ocean resources as perspective. All these applications require realistic driving functions, thus including accurate *P* estimates over wide ocean regions.

Consequently, the determination of the global hydrological cycle over the ocean has become a concern of prime importance to most fields of ocean and atmospheric sciences, and *P* has received an increasing attention in the last 15 years under of the World Climate Research Programme (WCRP), which frames the Global Energy and Water Cycle Experiment (GEWEX). This experiment studies the global freshwater budget, and carries out the Global Precipitation Climatology Project (GPCP, Huffman et al. 1997), with the objective to establish the best possible climatology of *P* at a global scale, over lands and oceans.

P is particularly patchy and intermittent, and due to both spatial and temporal scales at which *P* events occur, the estimation of a global *P* field is an extremely difficult exercise. Ways to estimate *P* rates over the sea have been reviewed in detail by the Working Group on Air–Sea Flux (WCRP-115 2001). Major sources of information are direct (or in situ) measurements, ship reports, satellite observations of several kinds, and Numerical Weather Prediction (NWP) centres, which have significantly improved the capability of their atmospheric models to produce reasonable estimates of *P*. As a consequence, several *P* data sets over the global ocean, built from one or a combination of the possible sources, are now available for periods longer than 10 years.

Inter-comparison projects have been carried out. The Algorithm Inter-comparison Program (Erbert et al. 1996) was an attempt to validate different satellite algorithms against in situ (rain gauges and radar) estimates. Therefore, attention was given to regional areas under different weather conditions. The Precipitation Inter-comparison Project (Adler et al. 2001), with the objective of improving satellite estimates, compared a set of monthly rainfall products. They showed the existence of large discrepancies among the products and proved the usefulness of combining multi-sensor observations with rain gauges. The main findings of these inter-comparison projects, which have been summarised in the WCRP-115 (2001) report, highlight the difficulty of selecting the best estimate, and there is still no recognised field of reference. However, the above studies, whose main objective was to improve satellite products, focused on short periods and gave little insight on long-term *P* climatologies.

Elements of comparison of *P* estimates over long periods can be found in several papers associated with the appearance of new climatologies (see Section 2.1 and Table 1 for a list of references). For example, Quartly et al. (1999) compared the spatial patterns of *P* in the Inter-Tropical Convergence Zone (ITCZ) using *P* climatologies derived from the TOPEX/POSEIDON satellite and GPCP. In fact, a double ITCZ is found in the two data sets in 1993–1996, which could be interpreted as an interannual signal (see Section 6.1). Estimates from TOPEX/POSEI DON are lower by 25% than GPCP values. Mean *P* field of the European Centre for Medium-range Weather Forecast (ECMWF) have been compared by Béranger et al. (1999) and Garnier et al. (2000) with the estimates provided by GPCP and those derived from the Comprehensive Ocean Atmosphere Data Set (COADS, Woodruff et al. 1987) by Da Silva et al. (1994) and Josey et al. (1999). These studies showed that ECMWF presents the highest value of *P* of all data sets, especially in the ITCZ and South Pacific

Convergence Zone (SPCZ), and pointed out an improvement of the re-analysis compared to the analysis. Other comparisons between GPCP and Climate Prediction Center Merged Analysis of Precipitation (CMAP, Xie and Arkin 1997) by Gruber et al. (1999) and Kidds (2001) show a good spatial and temporal correlation between GPCP and CMAP products in general. Nevertheless, GPCP estimates show higher P in the mid-latitudes and lower P in the tropics than those of CMAP. The use of different analysis procedures and of additional types of input data could explain the disagreement observed between estimates. However, these papers, which often focus on the production of a particular climatology, provide only a qualitative and piecewise view of the relative strengths and weaknesses between data sets.

All the above studies highlight the difficulty to determine the quality of the different data sets and speak in favour of continuous inter-comparison studies. It is the objective of the present study to carry out a quantitative inter-comparison of available global P climatologies, in an attempt to answer the following questions for which we have only very scattered elements:

- Are there any systematic differences between the various data sets according to their source (i.e. in situ, satellite, NWP, composite)?
- How well do the different available climatologies agree in their representation of the mean, of the seasonal cycle and of the interannual variability?

We approach the above questions from an ocean modelling perspective, in an attempt to provide information useful in selecting a P field as a component of the freshwater forcing of an OGCM. Therefore, the present analysis aims to reveal and document differences between various precipitation estimates, which are studied, but not to explain the reasons for these differences. Rather than comparing locally the details of the P fields, we compare the precipitation spatial average over pre-defined areas (called budgets hereafter) where the total amount of rain is suspected to have an impact on the ocean salinity. These areas are basically the major large-scale closed circulation features (ocean gyres).

We have selected ten different P data sets. Their sources, main characteristics and the period they cover are described in Section 2. Climatological annual means of each data set are compared in Section 3, and six data sets covering the same 14-year period (1980–1993) are retained for a quantitative analysis over specific ocean regions relevant to ocean main circulation patterns. Sections 4 to 6 are comparing these six selected data sets (UWM, SOC, ECMWF, NCEP, MSU and CMAP) over their common period. In Section 4, the climatological means are computed and compared. Differences are studied in terms of zonal averages, spatial patterns and regional P budgets. In Section 5, the climatological seasonal cycles (described in terms of climatological monthly mean anomalies) are studied. Then in Section 6, an analysis is undertaken to quantify how the different available data sets agree in their representation of the interannual variability. Again, the focus is on anomalies of the P budget over ocean regions of relevance to physical oceanography. Correlations between low-frequency time series of precipitation are investigated. In Section 7, the analysis of two other major data sets (HOAPS and GPCP), which do not cover the previous common 14-year period, is performed following the same methodology as before. A conclusion summarises the major findings of our comparison analysis and draws, whenever possible, quantitative statements on the strengths and weaknesses of the different data sets.

2 Precipitation data sets

P estimates over sea can be derived from three major sources which are (1) observations at sea (ship reports, ship and buoy measurements), (2) satellite observations and (3) forecasts carried out at NWP centres with atmospheric general circulation models. The reader is referred to the

Table 1 Characteristics of the various ocean precipitation data sets referenced in this study

Data Set	Reference	Period	Grid (deg)	Spatial coverage
Ships and buoys data				
CCR	Legates and Willmott (1990)	1950–1996	0.5	89.75°N–89.75°S
UWM	Da Silva et al. (1994)	1945–1993	1	89.5°N–89.5°S
SOC	Josey et al. (1999)	1980–1993	1	84.5°N–84.5°S
Satellite and rain gauge data				
TOPEX	Quartly et al. (1999)	1993–1999	5×2.5	70°N–67.5°S
HOAPS	Bauer and Schluessel (1993)	1992–1998	1	79.5°N–79.5°S
MSU	Spencer (1993)	1979–1993	2.5	58.75°N–58.75°S
Forecast: surface, meteorological, and satellite data with assimilation in NWP				
ECMWF	Gibson et al. (1997)	1979–1993	1.125	90°N–90°S
NCEP	Kalnay et al. (1996)	1958–1996	gauss 1.8	88.5°N–88.5°S
Satellite, rain gauge data or forecast (composite)				
CMAP	Xie and Arkin (1997)	1979–1999	2.5	88.75°N–88.75°S
GPCP	Huffman et al. (1997)	1988–1995	2.5	88.75°N–88.75°S

report WCRP-115 (2001) for a discussion of the various techniques and methods used to estimate *P*. The various *P* data sets or climatologies discussed in the present study are listed in Table 1, and their respective climatological annual mean is shown in Figs. 1 and 2.

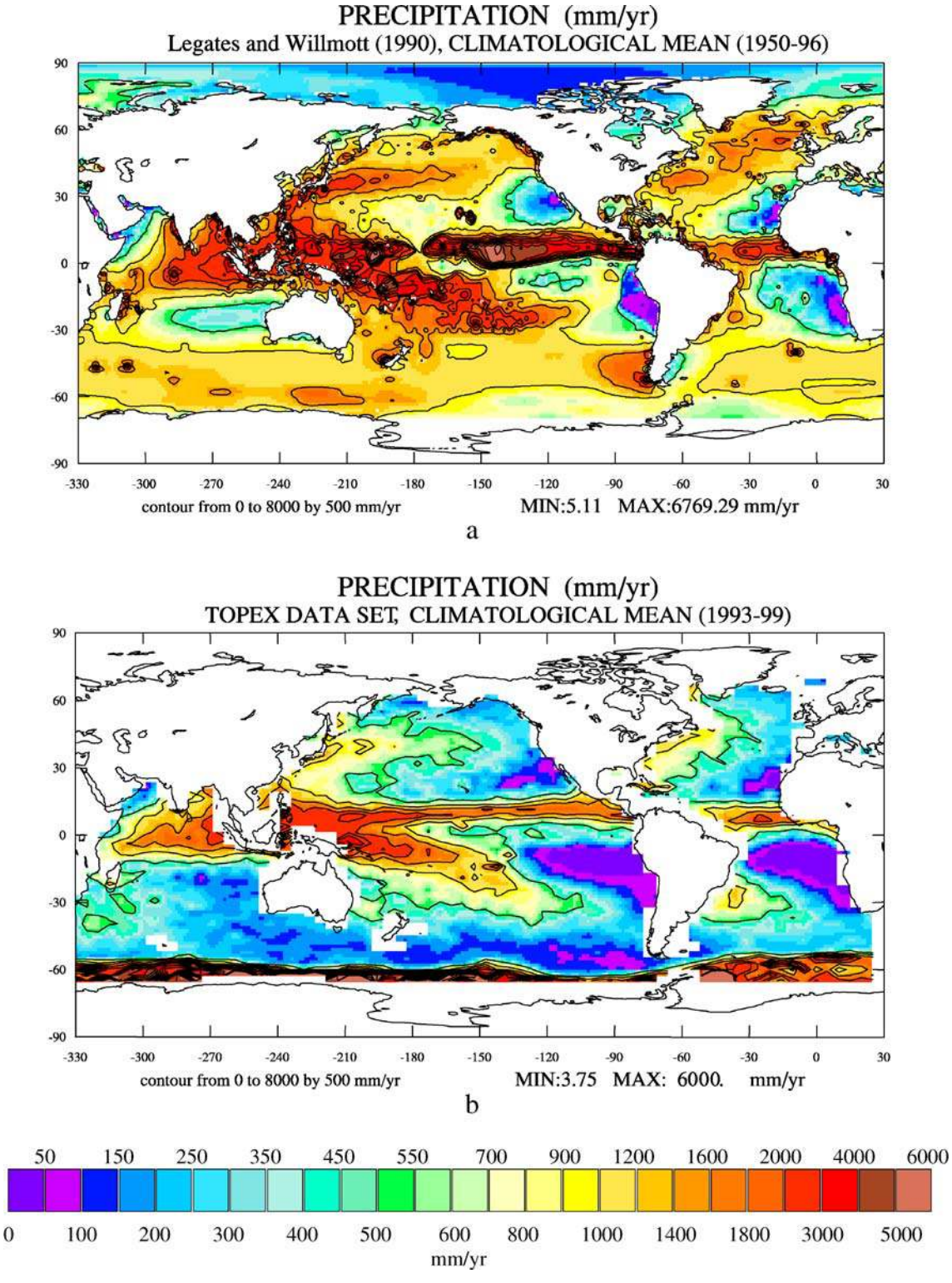

Fig. 1 Climatological mean precipitation over oceans for four data sets averaged over their whole record length. *Colours* indicate local values in millimetre per year. Contour intervals (in millimetre per year) range from 0 to 8,000 per 500. **a** The CCR data set (average from 1950 to 1996). **b** The TOPEX data set (average from 1993 to 1999). **c** The HOAPS data set (average from 1992 to 1998). **d** The GPCP data set (average from 1988 to 1995)

Fig. 1 (continued)

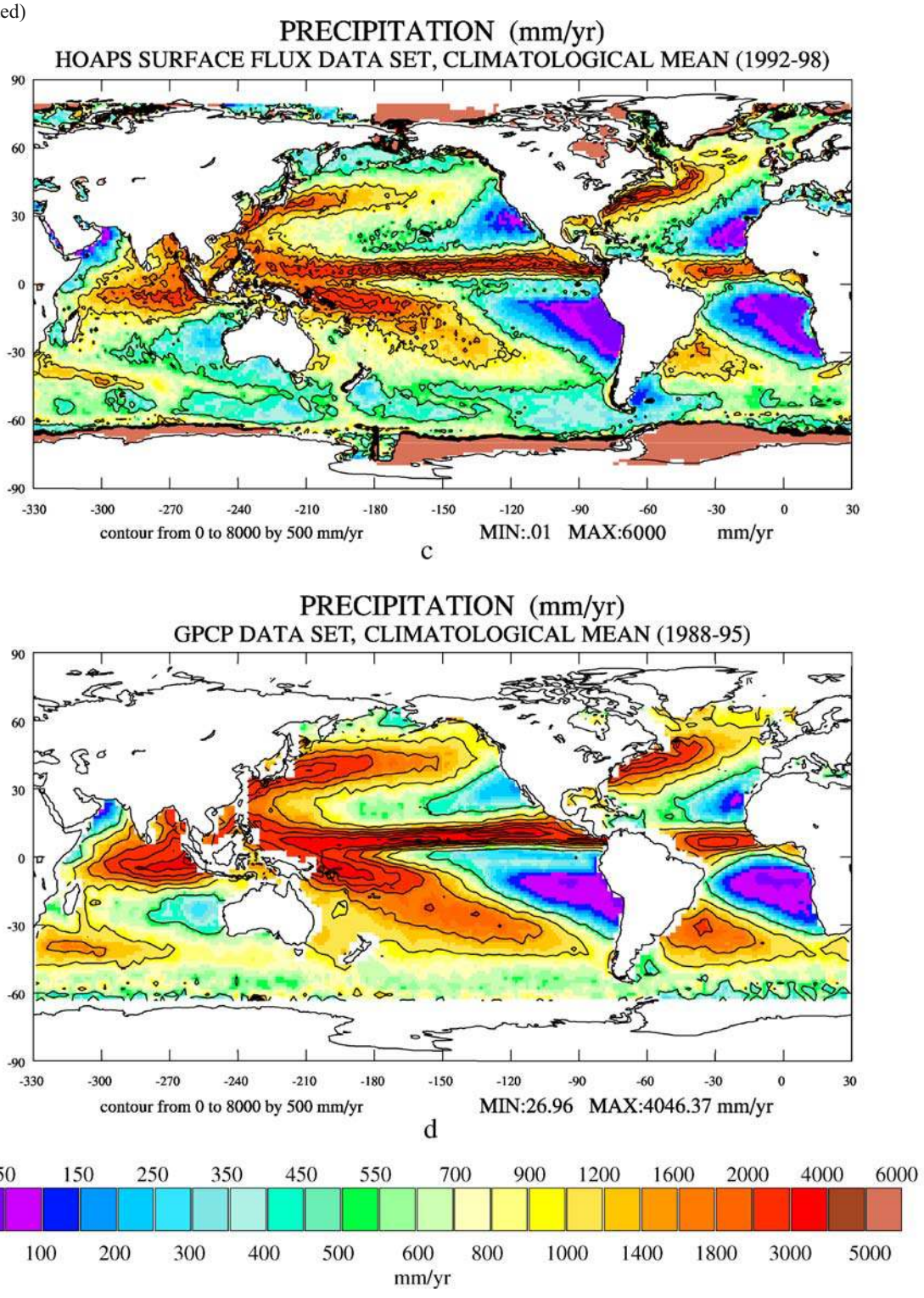

2.1 Precipitation data sets based on observations at sea

Local *P* estimates can be derived from ship reports (which do not measure *P* but report *P* conditions) or obtained from direct rain gauge measurements on ships and buoys (or radar on ship only). However, there are not enough direct measurements of *P* to establish a climatological (long-term) or a monthly mean over the global ocean, and a large recourse to ship reports is used.

The first global *P* climatology over lands and oceans was established by Baumgartner and Reichel (1975). Over land, runoff and *P* were based on direct hydrological measurements. Over oceans, very few data were available in the 1960s–1970s, and Baumgartner and Reichel constrained

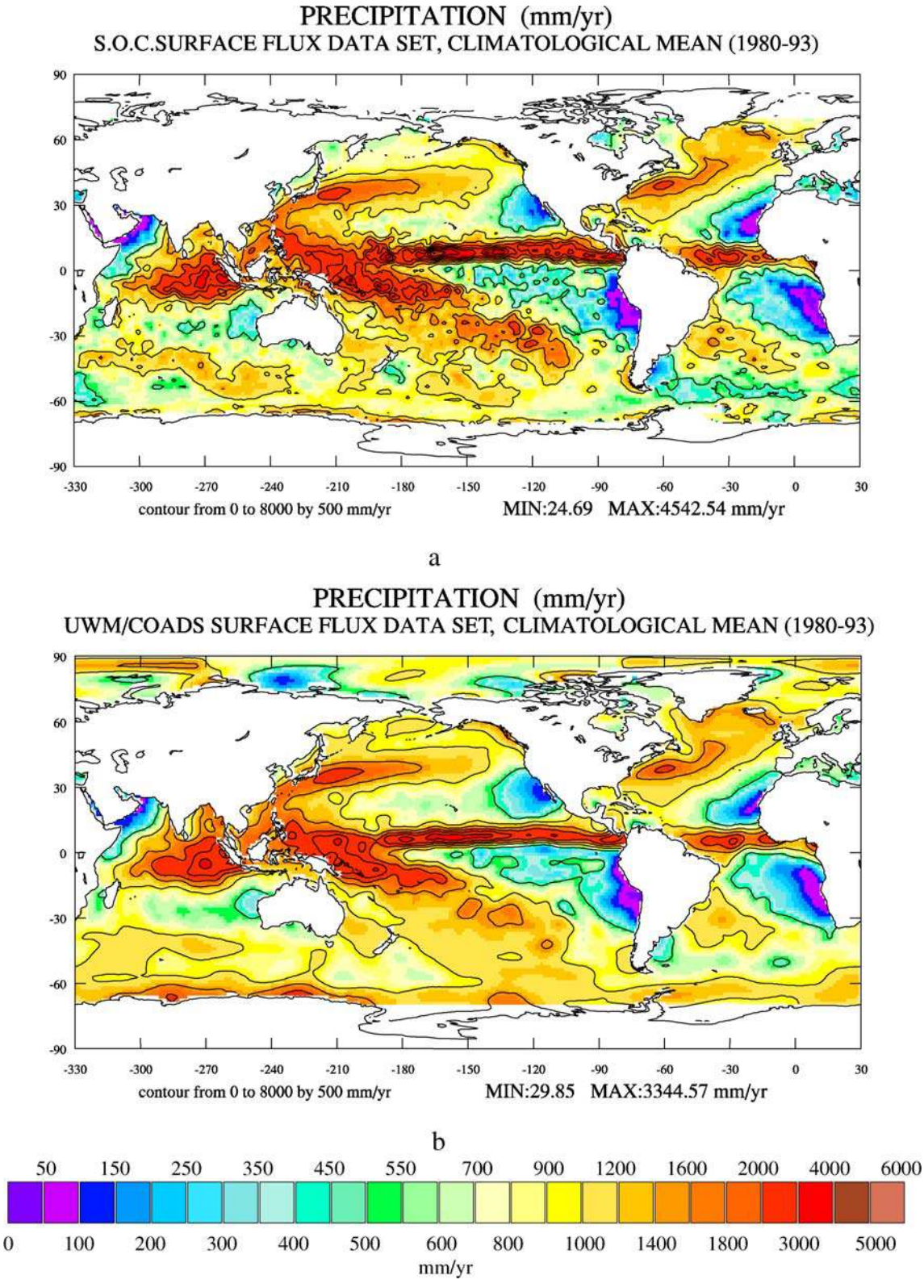

Fig. 2 Climatological mean (14-year average from 1980 to 1993) precipitation over oceans for six data sets having this period in common. *Colours* indicate local values in millimetre per year. Contour intervals (in millimetre per year) range from 0 to 8,000 per 500. **a** The SOC data set. **b** The UWM data set. **c** The MSU data set (lack of data in December). **d** The CMAP data set. **e** The ECMWF re-analysis data set. **f** The NCEP/NCAR re-analysis data set

Fig. 2 (continued)

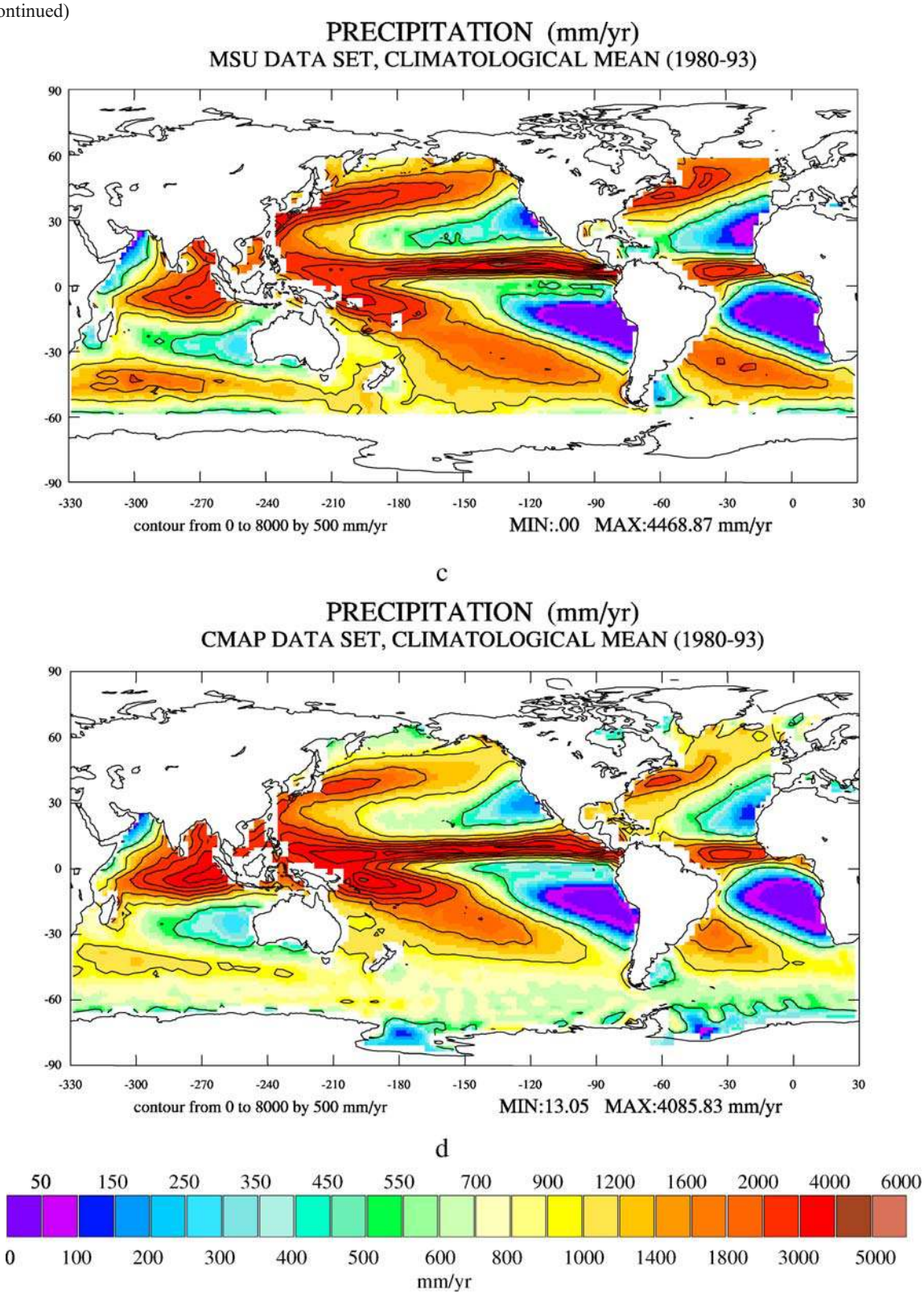

their ocean values with land values using a balanced freshwater budget. The main interest of this climatology over ocean lies in the balanced budget.

Recent ocean P climatologies, such as the three presented below, make a large use of COADS, which compiles almost all existing P measurements, and Volun-

Fig. 2 (continued)

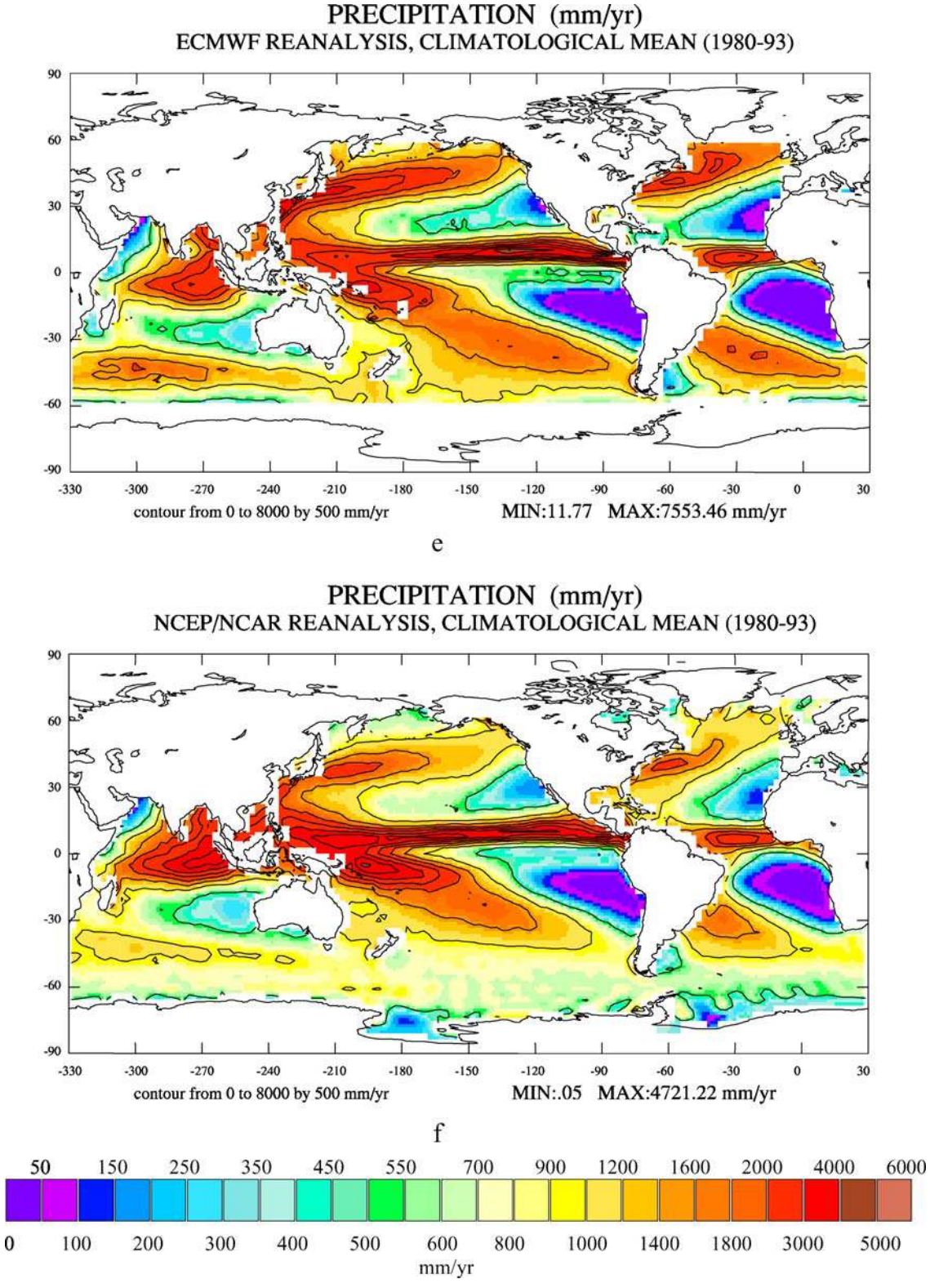

tary Observing Ship (VOS) reports for the last century. Precipitation estimates based on the VOS weather code may be influenced by the sampling errors, which consist of random sampling errors and fair weather bias. It has been pointed out that the fair weather bias may result in a systematic underestimation of the turbulent heat fluxes and wind speeds in case of stormy conditions (Gulev et al., submitted for publication). However, there is no clear

conclusion concerning the systematic or random character of the fair weather bias for precipitation.

CCR climatology Willmott and Matsuura at the Center for Climatic Research (CCR hereafter) extended the work of Legates and Willmott (1990) and proposed a climatology of *P* over ocean and land. Climatological monthly values were produced from a compilation of records obtained between 1950 and 1996 (http://climate.geog.udel.edu/~climate). Legates and Willmott have used the method developed by Tucker (1961). This method uses the present weather information of standard ship reports and relates it to precipitation rates according to a regression formula. Besides, in the tropics, an additional correction from Dorman and Bourke (1978) has been applied. To provide regular space coverage, the CCR climatology used an interpolated algorithm based on an enhanced distance weighting method and a neighbour-finding algorithm based on spherical distance.

UWM climatology A time series of monthly mean air–sea fluxes extending from 1945 to 1993 have been produced at the University of Wisconsin-Milwaukee (UWM hereafter) by Da Silva et al. (1994), in collaboration with the National Oceanographic Data Center and the National Oceanic and Atmospheric Administration. This analysis (Da Silva and White 1996) provides monthly *P* over the global ocean using surface observations or reports collected by ships and buoys.

SOC climatology Monthly air–sea flux estimates for the period 1980 to 1993 have been produced by Josey et al. (1999) at the Southampton Oceanography Centre (SOC hereafter). Flux estimates are obtained from in situ data, which are ship reports and buoy observations. Although using basically the same data as the UWM climatology, the processing is different. In particular, the radius of influence used in the interpolation method is smaller in the SOC analysis.

Both UWM and SOC climatologies were produced with a method of successive correction, a frequently used technique that is likely to introduce errors with irregularly sampled data. It does not require information about the temporal and spatial patterns of the fields. Data with different radii of influence are weighted by distance and averaged in successive passes of the smoothing process. This changes the characteristics of the data, degrades good measurements due to the overall lack of observations and creates a bias in the poorly sampled southern hemisphere due to southwards extrapolation of northern values. Thus, the quality of these estimates is considered as good in the northern hemisphere but poor in the southern hemisphere, particularly South of 30°S, where the number of observations considerably decreases and uncertainties on fluxes increase (White 1995; Glecker and Weare 1997). In this study, when we do not especially distinguish between SOC and UWM data sets, we refer to both of them as the COADS climatologies.

2.2 Precipitation data sets based on one kind of satellite observations

Satellite detection of *P* is likely to provide the best possible spatial and temporal coverage and is receiving strong support. An important difficulty is that space-borne sensors (radiometers or microwave radars) estimate an area-integrated quantity of water in the atmosphere rather than the actual rainfall, and thus provide precipitation rates different from those measured by pluviometers.

Another difficulty in satellite estimation of *P* resides in both spatial and temporal variability of this variable. Big cloud systems are few and small cloud systems are frequent and often last less than 1 h. Thus, to obtain a correct sampling remains a serious challenge. Several methods are being developed, which combine different sensors from different satellites (for a review, see Kidds 2001), and multi-sensor products are presently being improved. Four *P* climatologies are presently available, which use observations from a single satellite or combine different sources of data to construct an optimised estimate.

MSU climatology Monthly global *P* estimates based on Microwave Sounding Unit (MSU hereafter) measurements are available from January 1979 to May 1994 (Spencer 1993). A direct method is used, which consists in observing the effects of precipitating particles on radiation emitted by a radiometer at several frequencies. According to Spencer (1993), estimates in the extra-tropics are doubtful during the cool season. The MSU time series contains gaps due to the occurrence of failures in the retrieval of data, particularly in December over the whole 1980–1993 period. The MSU is insensitive to non-precipitating cirrus clouds and provides a robust signal in the tropics.

HOAPS climatology The Hamburg Ocean Atmosphere Parameters and Fluxes from Satellite (HOAPS hereafter) database provides *P* and fluxes obtained from processing Special Sensor Microwave Imager (SSM/I) and Advanced Very High Resolution Radiometer (AVHRR) (Bauer and Schluessel 1993). Indirect methods are used to retrieve the AVHRR data (radiometric observations in the visible and infrared), which catch the diurnal cycle. Recently developed methods have been applied and retrieval methods have been validated in comprehensive comparison studies with in situ measurements over the 1992–1998 period (Grassl et al. 2000). The HOAPS data set we worked with was not corrected for corrupted or spurious values. Precipitation values as large as 400 m/year were found in few places. Therefore, we masked the points where the climatological mean precipitation is above 9 m/year.

TOPEX climatology Estimates of *P* have been determined from dual-frequency altimeter radar measurements of the TOPEX/POSEIDON satellite (Chen et al. 1997; Quartly et al. 1999). Precipitation rates are bi-monthly values due to the sampling restriction of using a single altimeter and for a period extending from November 1992 to December 1999. This data set is referenced to as TOPEX hereafter. As for HOAPS, the TOPEX data set we worked with showed spurious values. The same masking (threshold of 9 m/year on the climatological mean) was applied.

2.3 Precipitation data sets based on NWP forecasts

Precipitation provided by weather forecasts carried out with atmospheric general circulation models at NWP centres remained very unrealistic for quite a time, mainly due to inaccurate cloud parameterisations. In fact, the low vertical resolution of the models did not allow describing narrow thermal inversions and then did not detect the strati-formed and cumuli-formed clouds, which are stopped under these inversions. Realistic inclusion of clouds with optical and convective properties in NWP models has been constantly improving in the 1990s, when new parameterisations were developed. Clouds of boundary layers were parameterised as a function of the intensity of the thermal inversion and of the humidity at the bottom of the inversion. Another improvement was to introduce a variable "liquid water rate". As a result of these new parameterisations and an increase in resolution, *P* forecasts considerably improved, and the monthly mean rain rates they produce became comparable to estimates from other sources.

The re-analysis projects carried out at the ECMWF and at the National Center for Environmental Prediction (NCEP) in collaboration with the National Center for Atmospheric Research (NCAR) provided long and consistent time series of *P* (and air–sea fluxes), which operational analyses could not provide due to continuous changes in the analysis/forecast system.

An analysis combines the output of a model forecast and observations (both relative to the same period of 6 h) to produce the state of the model that is the closest to the observations in an optimal sense (which depends on the data assimilation technique that is used). Therefore, the analysed fields are the prognostic model variables, which do not include the surface fluxes. In consequence, values of *P* are not obtained from the analysis, but are accumulated over forecast periods (from 6 to 24 h). Snowfall, large-scale and convective precipitation are included in the total *P*. It is worth mentioning that although many atmospheric observations of different kinds are assimilated in the model during the analysis, no *P* measurement is used during the forecast, so *P* is not constrained by any rain observation. Known problems of NWP forecasts are the representation of stratus clouds in regions of subsidence, and the excess of *P* during the model spin-up. The first re-analyses performed at ECMWF and NCEP are studied here. These meteorological centres have carried out second re-analyses, which are presently being evaluated.

ECMWF first re-analysis The re-analysis of ECMWF (ECMWF hereafter, Gibson et al. 1997) consists in an analysis carried out with a fixed state of the analysis/forecast system (the version of 1995), which includes a prognostic cloud scheme (Tiedtke 1993). The re-analysis was run for 15 years, from 1979 to 1993. Therefore, it presents a homogeneous record in comparison to operational analyses (Siefridt et al. 1999; Béranger et al. 1999). In this paper, we use the monthly mean of total *P* obtained from averaging the 12-h forecast (Garnier et al. 2000).

NCEP first re-analysis The NCEP/NCAR re-analysis (NCEP hereafter, Kalnay et al. 1996) consists in a re-analysis performed jointly by NCEP and NCAR (with the fixed NCEP analysis/forecast system as defined in 1995. This re-analysis runs for more than 40 years, from 1957 to present. Differences with the ECMWF re-analysis mainly reside in the atmospheric model and the assimilation process.

2.4 Precipitation data sets based on a combination of several satellite estimates, rain gauge observations or NWP forecasts

CMAP climatology The CMAP (Xie and Arkin 1997) produced a global *P* data set by merging rain gauge

Table 2 Annual period covered by the various precipitation data sets

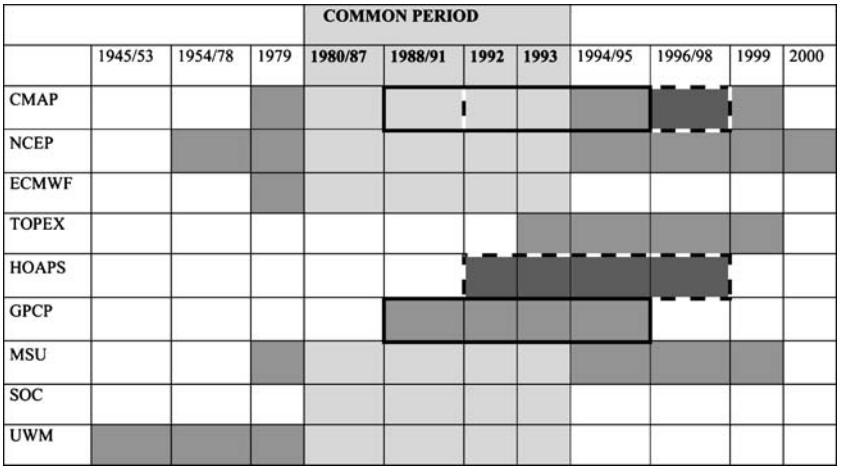

The period common to CMAP, NCEP, ECMWF, MSU, SOC, and UWM (14 years from 1980 to 1993) for which these six data sets are compared is shading in light grey. CMAP and GPCP are compared over the period 1988–1995 (thick dark frame). CMAP and HOAPS are compared over the period 1992–1998 (thick dashed frame)

measurements, *P* forecast from NCEP/NCAR re-analysis and five kinds of satellite estimates (CMAP hereafter). The CMAP product provides monthly means of *P* for the period from January 1979 to October 1999. In this study, CMAP will be considered mainly as a satellite product except at high latitudes (beyond 60°) where input from satellite becomes negligible. There, CMAP is basically equivalent to NCEP.

GPCP climatology A global monthly *P* data set for the period from July 1987 to December 1995 has been produced in the framework of the GPCP (Huffman et al. 1997). The analysis combines only rain gauge data from the Global Precipitation Climatology Centre (Rudolf et al. 1996), radiometer data from geosynchronous and orbiting satellites, and microwave data from the SSM/I. This data set is referenced to as GPCP in the following sections.

3 Overview of climatological mean *P* fields

Climatological mean *P* fields are displayed in Figs. 1 and 2 for the ten different data sets referred to in Table 1. Precipitation units used in this study are *millimetre per year* (*or millimetre per month*) *per unit surface of the ocean*, but are noted *mm*/*year* (or *mm*/*month*). Here, the climatological mean is the time average over the period 1980–1993 for the data sets which cover that period (SOC, UWM, MSU, CMAP, ECMWF, NCEP), and over their full record length for data sets which do not (CCR, TOPEX, HOAPS, GPCP). Note that for MSU, the annual climatological mean is only calculated with 11 months due to the lack of values in December over the whole period, which makes comparison with the other data sets inaccurate. The overview of climatological *P* fields presented in this section could be misleading because the analysis period of several data sets (especially HOAPS and GPCP) barely overlaps the period of 1980–1993 common to most other data sets. To avoid a misleading comparison, we also performed the analysis on the 1993 mean, which is common to almost all data sets (see Table 2), and verified that comments and conclusions relative to the comparison of climatological means are consistent with the analysis of the 1993 mean.

The comparisons of *P* maps (Figs. 1 and 2) demonstrate a qualitative agreement at the largest scales, contrasting regions of high and low *P* values. Precipitation is high in the ITCZ, the ascending branch of the Hadley Cell in the Atlantic, Pacific and Indian Oceans, and in the SPCZ. High values of *P* are also observed in the western part of the subtropical gyres, along the path of the warm western boundary currents. Regions of low *P* (<100 mm/year) are found in the eastern part of the tropical and subtropical ocean basins. For example in the descending branch of the Walker Cell, the quasi-constant subsidence of dry air limits convective phenomena, and rainfalls are particularly small in the eastern part of the subtropical ocean gyres. Quantitatively, the agreement between the various *P* estimates is generally poor. Differences between *P* fields can be locally very large, and before a detailed comparison is carried out (Sections 4 and 5), several examples of extreme discrepancies between *P* fields seen in Figs. 1 and 2 are pointed out in this section. Our comments are organised according to geographical areas defined in Fig. 3. The primary motivation for splitting the global ocean into regions is to perform regional budgets. Regions of Fig. 3 have been defined to idealistically represent the major large-scale ocean circulation features (i.e. eastern or western subtropical gyres, subpolar gyres, equatorial waveguide, the Southern Ocean). Precipitation budget (in the form of a spatial average) for a given region will thus be relevant to the salinity budget of the corresponding circulation feature.

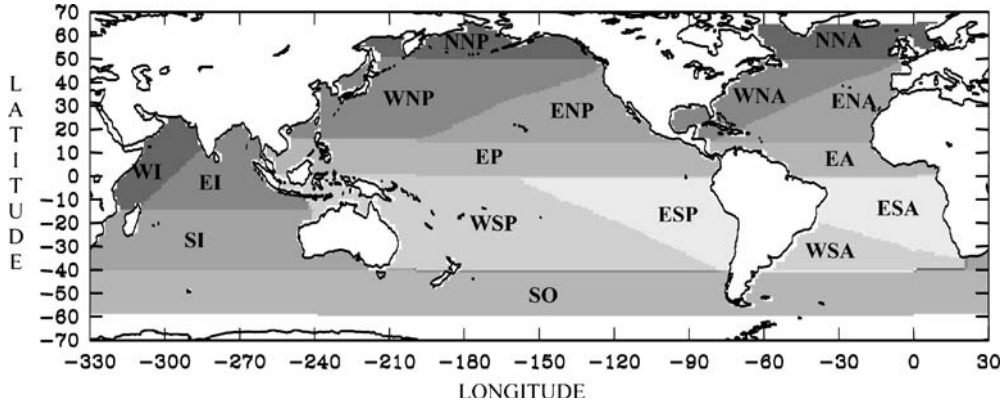

Fig. 3 Definition of 16 ocean regions for which precipitation budget has been calculated. Total precipitation over the region is calculated and normalised by the region area. These budgets are thus expressed in millimetre per year (or millimetre per month) per unit area. For convenience, mm/year (or mm/month) is used in the text and figures. *NNP* is the northern North Pacific region, *WNP* is the western North Pacific region, *ENP* is the eastern North Pacific region, *EP* is the equatorial Pacific region, *WSP* is the western South Pacific region, *ESP* is the eastern South Pacific region, *NNA* is the northern North Atlantic region, *WNA* is the western North Atlantic region, *ENA* is the eastern North Atlantic region, *EA* is the equatorial Atlantic region, *WSA* is the western South Atlantic region, *ESA* is the eastern South Atlantic region, *WI* is the western Indian region, *EI* is the eastern Indian region, *SI* is the southern Indian region and *SO* is the Southern Ocean region

3.1 Equatorial oceans

In the equatorial Pacific (EP in Fig. 3), mean *P* values range for most data sets from 2,000 to 3,000 mm/year, except for TOPEX (1,000 to 1,500 mm/year only) and CCR and ECMWF (over 4,000 mm/year). In addition, CCR shows a much broader ITCZ with a discontinuity near 180°W that is probably due to a lack of data.

In the equatorial Atlantic (EA in Fig. 3), *P* means range between 1,500 and 2,500 mm/year, except in TOPEX and HOAPS where they are less than 1,000 mm/year.

In the eastern Indian (EI in Fig. 3), *P* values range in the Gulf of Bengal between 2,000 and 3,000 mm/year from one data set to another, except for TOPEX and HOAPS, which again exhibit the lowest values (about 1,500 mm/year).

The western Indian (WI in Fig. 3) is characterised by a great *P* contrast between the Arabian coast (a dry area) and the coast of the Indian Peninsula (a wet area) as seen in all data sets.

3.2 Western tropical and subtropical oceans

In the western North Pacific (WNP in Fig. 3), *P* maxima are localised along the path of the Kuroshio Current. Highest values of *P* are found in MSU and GPCP (2,500 mm/year), almost 500 mm/year more than other data sets, whereas TOPEX (800 mm/year) and HOAPS (1,000 mm/year) present the lowest values.

The major *P* pattern of the western South Pacific (WSP in Fig. 3) is the SPCZ and is differently represented in the various data sets. The maximum of *P* is located to the East of New Guinea. ECMWF has the greatest value among all data sets there, with more than 4,000 mm/year, twice the value proposed by TOPEX or COADS (2,000 mm/year). HOAPS is also lower than average there, with only 2,500 mm/year. The poleward extent of the SPCZ is similar between all data sets except CCR. From its *P* maximum off New Guinea, the SPCZ extends to the Southeast to about 45°S-100°W, and exhibits a secondary *P* maximum at 30°S-150°W clearly separated from the one off New Guinea in some data sets. Maximum *P* values found there vary from 1,400 to 2,000 mm/year, according to the data set considered. In CCR, the extent of the SPCZ is limited to 30°S (a consequence of the limited number of observations South of this latitude).

In the western North Atlantic (WNA in Fig. 3), *P* maximum is localised along the path of the Gulf Stream and the North Atlantic Current, where values range from 500 to 1,500 mm/year. Differences between data sets are similar to those noted above in the western North Pacific. The maximum of *P* (1,500 to 2,000 mm/year) in this region closely follows the path of the Gulf Stream in every climatology except for TOPEX. The spatial distribution of *P* in this region, however, is similar between NWP's and satellite-derived products (except TOPEX).

In the western South Atlantic (WSA in Fig. 3), all satellite products except TOPEX and HOAPS (i.e. GPCP, MSU, CMAP) provide by far the largest *P* values.

3.3 Eastern tropical and subtropical oceans

These regions (identified by ENP, ESP, ENA, ESA and SI in Fig. 3) are characterised by a strong atmospheric subsidence associated with very low precipitation. Large areas of *P* rates under 50 mm/year are found in eastern mid-latitude ocean basins in all data sets, except those derived from observations at sea (i.e. CCR, SOC and UWM). In those latter data sets, the smallest *P* values are above 50 mm/year. The extent to the West of these areas of low precipitation appears to be similar among most satellite products (CMAP, MSU, GPCP, HOAPS), but does vary quite significantly between the other data sets.

3.4 Southern ocean

Data sets appear to agree with regard to the spatial distribution of precipitation in the Southern Ocean (SO in Fig. 3). This region is limited to 60°S in our study because most data sets do not provide *P* estimates beyond this latitude. A band of high *P* is found in the Indian sector of the Southern Ocean, along the eastward extension of the return flow of the Agulhas Current. Elsewhere, the Antarctic Circumpolar Current is characterised by rather uniform *P*. Large *P* is found confined along the coast of Chile (upwind of the Andes) and low *P* East of South Argentina (downwind of the Andes). Again, differences between data sets are mainly quantitative, but are quite large. TOPEX presents *P* rates, which seem abnormally small (below 150 mm/year almost everywhere). HOAPS also presents small *P* values, but they are generally above 300 mm/year. Other data sets show values from 500 mm/year to above 1,000 mm/year in the Antarctic Circumpolar Current (more than 100% difference).

3.5 Remarks

Spatial patterns and magnitude of *P* over oceans are very differently reproduced by the data sets discussed here. Two particular data sets, TOPEX and CCR, appear to be especially far from the others. In particular, TOPEX does not reproduce several important patterns of *P* that all other satellites do. A significant amount of precipitation does fall in light events and the inability of TOPEX to detect them may explain part of the observed deficiencies. The same remark holds in extra-tropical bands, where other satellite-based estimates of *P* are twice greater than for TOPEX. CCR shows unrealistic local extremes, characteristic of an inadequate smoothing method to account for the lack of data and the irregular sampling (see Section 2.1).

The qualitative analysis carried out above demonstrates that local values of P may differ significantly (by more than 100% in very specific areas) from a data set to another. However, it is difficult with such a visual analysis of global maps to clearly identify systematic differences between the various data sets according to their source.

Eastern subtropical gyres (i.e. regions of P minimum) are regions where such systematic differences are noticeable. Satellite products exhibit the areas of low P of greatest extent, whereas in situ (i.e. COADS-derived) products show the smallest, likely due to the poor sampling of central tropical oceans (especially in the southern hemisphere) by ships from the Voluntary Ocean Ship program. NWP products seem to lie in between.

However, it is the integrated value of P rather than its local value which matters for the salinity budget of ocean circulation patterns. Therefore, the mean and variability of the budget of P in regions relevant to ocean dynamics (see Fig. 3) are studied in the next four sections, an approach that allows quantitative comparisons.

If we expect to find geophysical signals or trends and to point out artificial bias in the various data sets, their comparison must be performed over a common period. According to Table 2, six of the ten data sets have 14 years in common during 1980 to 1993, distinguishing between the three major sources of P estimates: in situ (i.e. COADS) derived data sets with SOC and UWM, NWP products with ECMWF and NCEP, and satellite products with MSU and CMAP. In the following three sections, we shall concentrate on these particular data sets, over this particular 14-year period. HOAPS and GPCP will then be studied separately over the period each has in common with CMAP (Section 7).

4 Climatological mean (1980 – 1993)

In this section, we proceed to a quantitative comparison of the climatological mean P estimates provided by the six data sets covering the 1980–1993 period. The 14-year (i.e. climatological) mean P fields relative to these data sets are shown in Fig. 2 and were qualitatively compared in the previous section. First, these mean fields are compared from their zonal average. Then, area averages of precipitation are calculated for 16 oceanic regions (Fig. 3). These spatial averages, which are called regional budgets hereafter because they are related to the total amount of precipitation in the region, are quantitatively compared.

4.1 Zonal average of annual mean precipitation

In a first attempt to quantify the differences between the various precipitation climatologies, we compare their zonal average noted $\overline{P}$ (Fig. 4). As in many other studies (White 1995; Béranger et al. 1999; Gruber et al. 1999; Adler et al. 2001; Kidds 2001), the 10°S–10°N latitude band is where precipitation is the largest and where largest disagreements occur.

Although all data sets place the $\overline{P}$ maximum of the ITCZ around 6.5°N, the value of the maximum differs quite a lot from one data set to another. The difference between the two NWP products is extremely large, with ECMWF showing the greatest value (3,222 mm/year) of all data sets and NCEP nearly the smallest (2,206 mm/year). This represents a discrepancy of 30%. The satellite products CMAP (2,817 mm/year) and MSU (2,507 mm/year) also present high $\overline{P}$ values but differ by only 310 mm/year

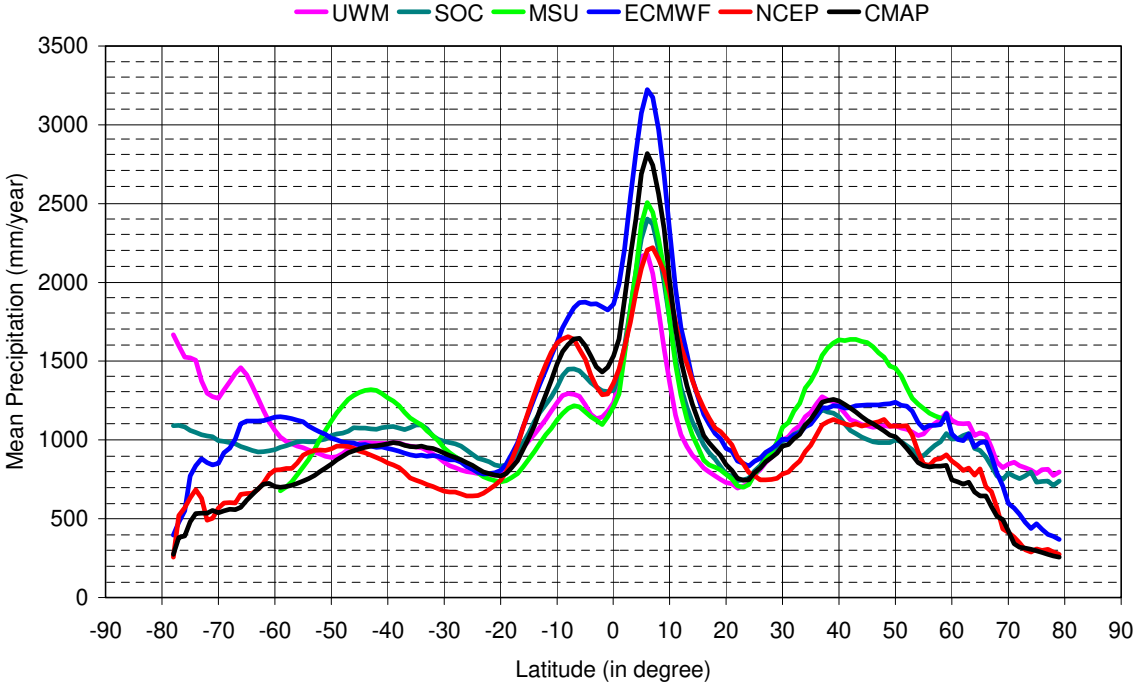

Fig. 4 Zonal average of climatological mean (14-year mean from 1980 to 1993) precipitation over the global ocean for the six data sets, which have this period in common

(≈12%). In situ products SOC (2,402 mm/year) and UWM (2,180 mm/year) are those showing the better agreement since their difference barely exceeds 220 mm/year (≈10%).

Large disagreements between data sets are also found at the latitude of the SPCZ (between 5 and 8°S). The value of $\overline{P}$, provided there by ECMWF, is again significantly above all the other estimates (1,875 mm/year), but NCEP value of $\overline{P}$ is now among the highest (1,654 mm/year), so the discrepancy between the two NWP products (12%) is not as large as for the ITCZ. The discrepancy between the two satellite products is drastically increased at this latitude. Whilst CMAP estimate of $\overline{P}$ remains among the highest (1,646 mm/year), the one from MSU falls last (1,217 mm/year), revealing a discrepancy of 25% (against 12% in the ITCZ). Agreement between the in situ products is again rather good because their difference remain of the order of 10% at this latitude. Note that in this band of latitude, the agreement about the place of maximum $\overline{P}$ is not as good as for the ITCZ. ECMWF and CMAP place it at 5.5°S, NCEP at 7.5°S, and it is placed at 6.5°S in the other climatologies.

All data sets converge to more comparable values in regions of low precipitation. In the southern tropics at 20° S, the difference between the highest value (i.e. SOC with 840 mm/year) and the lowest value (i.e. NCEP with 711 mm/year) does not exceed 15%. The same is noticed in the northern tropics at 24°N. As expected from the distribution of *P* shown in Fig. 2, in situ products (i.e. SOC and UWM) are those which exhibit the highest values in zonal average at the latitudes of the southern tropics (20°S), in relation to their smaller extent of regions of *P* minimum in the East of the ocean basins (see Section 3.5). Note that NCEP places the tropical minimum of $\overline{P}$ at higher latitudes than the other data sets. For the southern minimum (placed at 24.5°S instead of 20°S), this is due to a more zonal pattern of the SPCZ, which has a lesser poleward extent in the South Pacific, and a stronger *P* minimum in the East of the southern Indian (see Fig. 2). For the northern minimum (placed at 27.5°N instead of 22.5°N), this is likely due to the band of low *P* found between 28 and 30°N all across the Pacific Ocean (see Fig. 2).

In subtropical and subpolar regions (from 30° to 60° latitude in both hemispheres), MSU estimate of $\overline{P}$ (1,634 mm/year at 40°N) is well above all other estimates (which all agree within 5% or better of their average value of 1,187 mm/year at this latitude). This large overestimation of *P* in the MSU data set is also obvious in Fig. 2. NCEP provides smaller values of $\overline{P}$ than other data sets in subtropical gyres (about 200 mm/year less than ECMWF), which reveal smaller *P* over the warm western boundary currents (see Fig. 2).

Divergence between data sets increases again at latitudes higher than 60°. However, we do not comment on the respective behaviour of the various data sets for several reasons. Satellite product does not provide reliable values of *P* beyond 60°. So there is no available estimate for MSU and CMAP, which is a composite product similar to NCEP at high latitudes where the input from satellite is reduced. In situ estimates of *P* are not reliable at high latitudes because of a lack of observations in both hemispheres, although this is more crucial in the South. Therefore, our comparison is limited to NWP products. ECMWF and NCEP show a similar behaviour in zonal average in the northern hemisphere (ECMWF being roughly 200 mm/year greater than NCEP). They are very different in the Southern Ocean, with NCEP showing a continuous poleward decrease of $\overline{P}$ starting at 50°S, whereas in ECMWF, $\overline{P}$ increases continuously from the tropics to 65°S before showing a sharp decrease at higher latitudes.

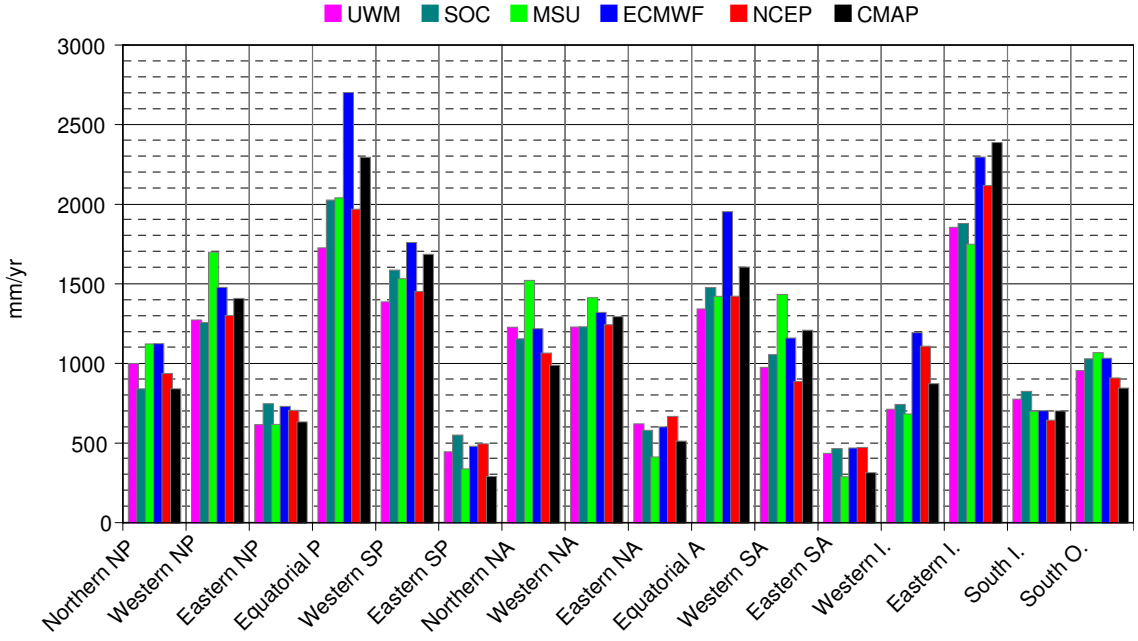

Fig. 5 Spatial average of the mean (1980–1993) precipitation (in millimetre per year) for every ocean region defined in Fig. 3. The six data sets, which have in common the 1980–1993 period, are plotted

4.2 Spatial patterns and regional budgets

The comparison of the climatological mean precipitation provided by the six selected data sets is continued by looking at regional budgets (i.e. area averages) calculated over the 16 oceanic regions defined in Fig. 3. Each region is relevant to ocean circulation patterns for which the total amount of precipitation is important for the salt budget. These regional budgets of *P* are shown in Fig. 5. Our analysis also makes use of the spatial patterns of *P* associated with each region as they appear in Fig. 2.

4.2.1 Equatorial regions of high precipitation

Equatorial pacific This area (EP in Fig. 3) is marked by the band of high precipitation associated with the ITCZ along the equator (see Fig. 2). Within this band, a maximum in *P* is found to stretch across the central Pacific (120°W to 180°W) in all data sets, except in NCEP where the *P* maximum is clearly placed in the western Pacific (180°W to 240°W). In fact, all data sets exhibit some kind of maximum of *P* in the western Pacific, as well seen in ECMWF and CMAP and barely noticeable in MSU. Highest local values of *P* above 4,000 mm/year are found in several places in ECMWF and in one spot of the central Pacific in SOC and in MSU (not in the same place).

The precipitation budget of the EP box (Fig. 5) shows that SOC, MSU and NCEP estimate the area-averaged precipitation in the equatorial Pacific to a value close to 2,000 mm/year, despite the different origin of the data. ECMWF and CMAP, with a budget of 2,600 and 2,300 mm/year, respectively, provide quite a large and likely unrealistic amount of precipitation in the equatorial Pacific. UWM shows the lowest budget with 1,700 mm/year.

Equatorial Atlantic The pattern of the band of high precipitation associated with the ITCZ in the equatorial Atlantic is quite different according to the origin of the data sets (see Fig. 2). In the satellite products MSU and CMAP, the maximum of *P* is placed in the central Atlantic near 30°W. In situ products SOC and UWM also place the maximum *P* at 30°W, but also show an increase of *P* at 10°W along the coast of Sierra Leone. In NWP data sets, two maximum of *P* are seen, the higher being placed in the West and the lower in the East. ECMWF exhibits the greatest values of *P*. All data sets more or less show an increase of *P* in the Gulf of Guinea.

Despite these significant differences in precipitation patterns, most climatologies propose a very comparable budget over the equatorial Atlantic. The area average of *P* is around 1,400 mm/year for all data sets, except for CMAP (1,600 mm/year) and ECMWF (1,900 mm/year).

Eastern Indian The tropical part of the Indian Ocean (i.e. North of 20°S) is characterised by a strong East–West precipitation contrast (see Fig. 2). The eastern part of this basin (EI in Fig. 3) is under the influence of the Indonesian atmospheric rise and is a place of high precipitation. In all data sets but NCEP, *P* maximum is placed off Sumatra and stretches westward, highest *P* occurring South of the equator. In NCEP, the coast of Sumatra is characterised by a relative minimum in *P* (1,000 mm/year lower than values around), which stretches westward along the equator, separating two areas of *P* maximum in the Gulf of Bengal to the North, and in the central Indian Ocean to the South. In situ products SOC and UWM have the lowest *P* estimates in the Gulf of Bengal among all data sets.

In terms of budget, this is the region of second highest precipitation after the equatorial Pacific (see Fig. 5). The in situ products SOC and UWM have very comparable budgets, each showing an area-averaged *P* of nearly 1,800 mm/year. The ECMWF again shows large area-averaged *P* (≈2,300 mm/year, nearly 200 mm/year more than NCEP); it is the CMAP climatology, which has the largest *P* budget (≈2,400 mm/year). The MSU climatology shows the smallest budget from all data sets (1,700 mm/year).

4.2.2 Tropical and subtropical regions of high precipitation

Western North Pacific This region (WNP in Fig. 3) comprises the China Seas and the Kuroshio Current. Whereas most data sets show comparable patterns of precipitation in this area (see Fig. 2), the MSU climatology shows a clear bias towards high *P* values, particularly in the region of the Kuroshio. In the area-averaged budget over the WNP region (Fig. 5), MSU reaches 1,700 mm/year, the greatest value among data sets. SOC, UWM and NCEP agree on a budget of nearly 1,300 mm/year. The area-averaged precipitation of CMAP (≈1,400 mm/year) and ECMWF (barely below 1,500 mm/year) are again on the side of the high estimates.

Western South Pacific This region (WSP in Fig. 3) includes the SPCZ, the influence of which on the area-averaged budget is dominant. The pattern of the SPCZ (Fig. 2) is the more zonal in NWP products. It has a greater extent to the Southeast across the Pacific in satellite estimates (it almost goes across in MSU), and appears as two separated regions of high *P* in the COADS derived climatologies.

In terms of budget (Fig. 5), this region is very similar to other regions of tropical convergence (EP and EA in Fig. 3), with ECMWF and CMAP showing greater area-averaged values.

Western North Atlantic This region includes the Gulf of Mexico and the Gulf Stream current systems (WNA in Fig. 3). MSU climatology shows a clear bias towards high *P* values in the region of the Gulf Stream (see Fig. 2). Other data sets show comparable patterns of precipitation in this area. The area-averaged budget over the western North Atlantic is 1,500 mm/year for MSU, the greatest value among data sets. Other data

sets agree (within a few percent) on a budget of nearly 1,200 mm/year, with again ECMWF showing the largest value (1,300 mm/year).

Western South Atlantic The region (WSA in Fig. 3) is characterised by a pattern of high *P*, which extends over the Brazil current system and its eastward extension. Satellite estimates are greater than all the others (Fig. 2), MSU being the greatest, by far. Therefore, MSU and CMAP show the largest budgets (Fig. 5) with 1,400 and 1,250 mm/year, respectively. Contrary to the northern subtropical gyres (WNP and WNA), differences are large between data sets in pattern as in budget (850 mm/year for NCEP and 1,150 mm/year for ECMWF the other NWP product).

4.2.3 Tropical and sub-tropical regions of low precipitation

Regions of atmospheric subsidence In Fig. 3, regions of atmospheric subsidence are the eastern North and South Pacific (ENP and ESP), and the eastern North and South Atlantic (ENA and ESA). There is an obvious consistency between data sets of same origin. SOC and UWM show very alike *P* patterns (Fig. 2) and present a reasonable agreement on the budget, *P* being usually greater in SOC except in the ENA (Fig. 5). The same comment goes for NCEP and ECMWF, with *P* being usually greater in NCEP except in the ENP. MSU and CMAP satellite *P* estimates provide the largest areas of very small precipitation, which is revealed in lowest budget values in Fig. 5.

Western Indian The Arabian Sea (WI in Fig. 3) is a region of small precipitation. In SOC, UWM and MSU, the *P* minimum is seen along the Arabian Peninsula (Fig. 2) and stretches southward along Somalia to reach Madagascar. Local values of *P* and area-average budgets are very similar between these three data sets (agreement is better than 5%, Fig. 5). The three other climatologies (ECMWF, NCEP and CMAP) show much greater *P* budgets (1,250 mm/year in ECMWF against 700 mm/year for MSU) due to the westward extent of the *P* maximum in the equatorial Indian in the Mozambique Channel. Discrepancies can reach 40% in area averages over the region between data sets, with NWP products showing the largest values.

Southern Indian The subtropical gyre of the Indian Ocean (SI in Fig. 3) is characterised by quite low precipitation in the East (Fig. 2). The *P* minimum off Australia is most marked in NCEP, which also presents the smaller area-averaged budget (650 mm/year). This minimum is not as well seen and does not extend as far to the West in in situ *P* estimates (SOC and UWM), which consequently exhibit the highest budget (750 to 800 mm/year). However, the general agreement between the data sets is better than 20% on the area-averaged budget (Fig. 5), so the southern Indian is a region where the various *P* estimates are in a relatively good agreement on the climatological mean.

4.2.4 High latitudes regions

Northern subpolar gyres Agreement between data sets of the same source is poor on the *P* budgets (Fig. 5) of the northern North Pacific and the northern North Atlantic (respectively, NNP and NNA in Fig. 3). As already mentioned, CMAP and NCEP become similar at high latitudes when the weight of satellite data in the CMAP estimate becomes insignificant. In the northern North Pacific, SOC is 20% higher than UWM, as is ECMWF compared to NCEP, and MSU is 30% larger than CMAP. These discrepancies are reduced to 10% in the northern North Atlantic for in situ and NWP products, which show comparable budgets. On the contrary, the *P* estimate by MSU in the North Atlantic subpolar gyre is 30 to 40% above the others. NCEP (and consequently CMAP) is with SOC, the only data set to propose *P* values below 1,000 mm/year in the Aleutian low-pressure system.

Southern Ocean The Southern Ocean (SO in Fig. 3) is comprised between 40 and 60°S, because the validity of the data sets beyond 60° latitude, particularly in situ and satellite products, is questionable. As for the subpolar regions of the northern hemisphere, CMAP is equivalent to NCEP. The distribution of *P* (Fig. 2) shows the highest values in the Indian sector, and from there, *P* continuously decreases across the Pacific sector and is minimum in the Atlantic sector. All data sets qualitatively agree with this distribution. However, ECMWF places the Indian *P* maximum at 58°S, whereas every other data set places it between 45 and 50°S. This high *P* is much greater in MSU. ECMWF estimates are generally the highest. Note that regional minima along the southwestern coast of Argentina and at the east of New Zealand are well seen in all climatologies, as is the local maximum south of Chile.

The area-averaged budget (Fig. 5) ranges between 800 mm/year for the smallest estimate (CMAP) and 1,100 mm/year for the largest (MSU), for a 30% scatter.

In situ products seem in agreement with each other, as their discrepancy does not exceed 100 mm/year (or 10%) over the whole area. Discrepancy between NWP products is again over 20%.

4.2.5 Remarks

The analysis of the climatological mean of the six data sets covering the same 14-year period has demonstrated that large discrepancies exist between data sets, which cannot generally be attributed to the origin of the data (i.e. in situ, satellite or NWP), although in some regions, a generic bias may exist.

Two important *P* data sets, HOAPS and GPCP, were not part of the above analysis because they cover a different period.

The climatological mean *P* of GPCP (Fig. 1) seems in agreement with CMAP (Fig. 2) with similar patterns and smoothing, although it shows greater values in western subtropical gyres and in the central equatorial Pacific. The two products are very alike and a comparison over their common period (Gruber et al. 1999) showed a good spatial and temporal correlation between them, except in the tropics. HOAPS *P* estimate is a satellite product very

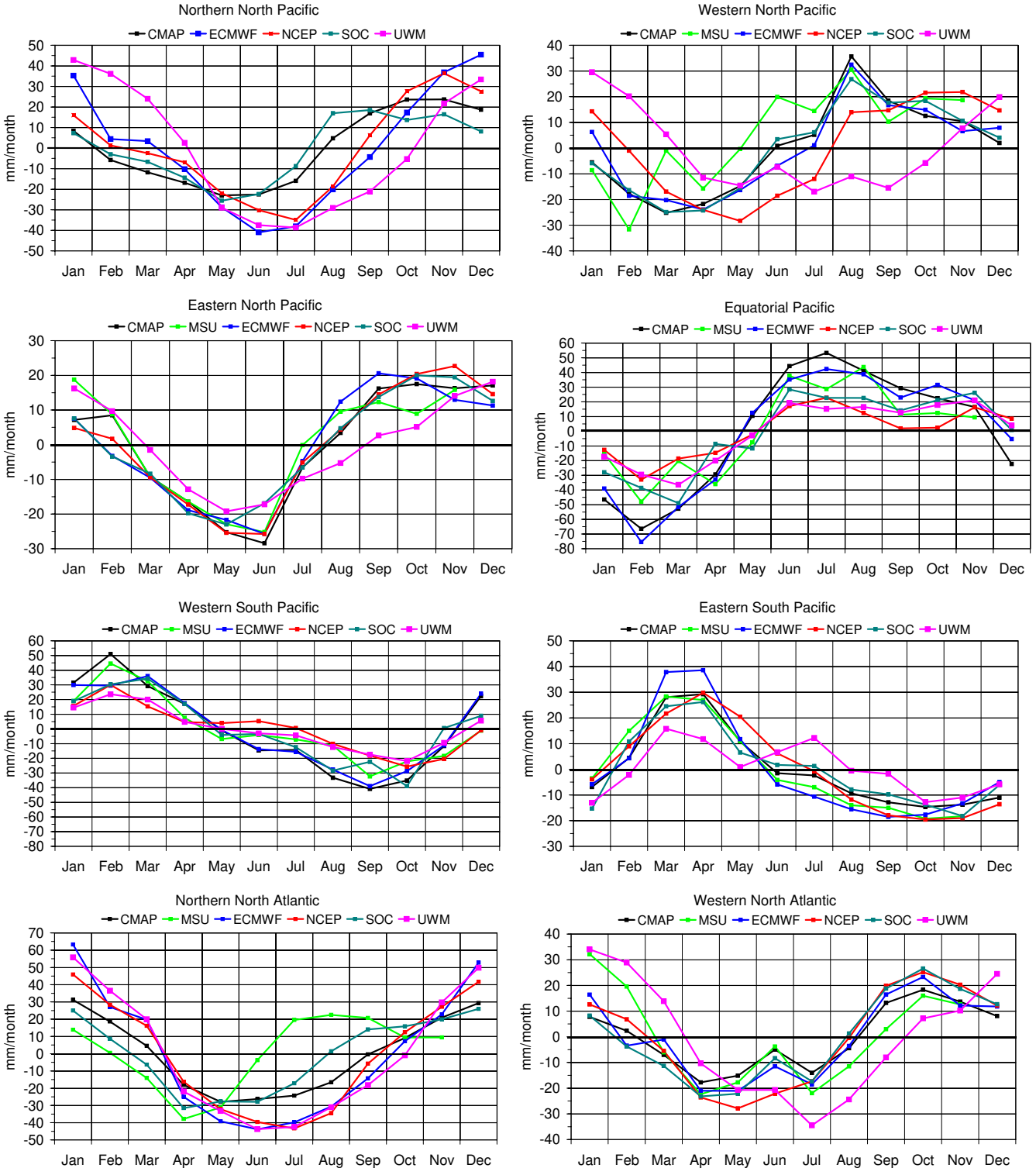

Fig. 6 Climatological seasonal cycle of precipitation (i.e. monthly mean precipitation anomalies) for the 16 ocean regions defined in Fig. 3, for the six data sets, which have in common the 1980–1993 period. The climatological annual mean (1980–1993 mean) for each data set has been subtracted to the climatological monthly means, and a spatial average over the region was performed. There were not enough MSU data in the NNP to provide a seasonal signal

Fig. 6 (continued)

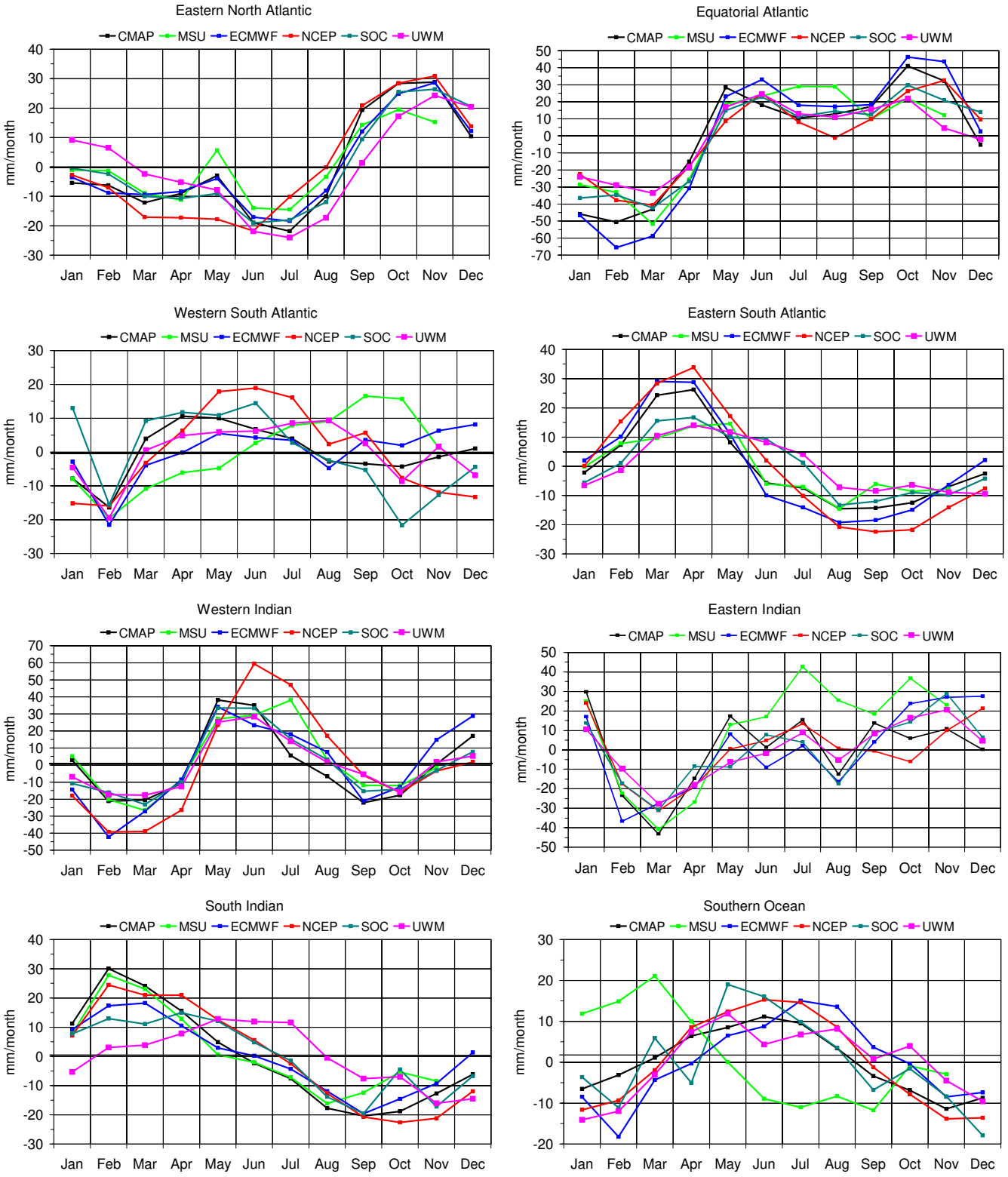

different from any other data sets. Compared to other satellite products and even to NWP products, HOAPS is remarkable by its high resolution (Fig. 1). It resolves smaller *P* features and shows greater *P* contrasts. A finer band of high *P* in the equatorial Pacific, a finer definition of the patterns of high *P* in the western boundary currents (as in the Agulhas Current and the Gulf Stream), pools of low *P* in the Indian and Pacific sectors of the Southern Ocean (east of New Zealand and over the Argentinian shelf for example) and the pool of low *P* in the Mozambique

Channel suggested, but not resolved by most of the other data sets, are the most remarkable features, and a well-defined region of low P is the Pacific subtropical gyre. The reality of these fine patterns are often suggested in in situ or other satellite products, which cannot resolve it due to averaging or smoothing. However, their quantitative significance has to be discussed. The comparison of HOAPS and GPCP with CMAP over their respective common periods is presented in Section 7.

5 Seasonal variability

In this section, we make a comparison of the climatological mean seasonal cycle of the P estimates provided by the six data sets covering the common 14-year period 1980–1993. We focus on the area averages (over the 16 regions of Fig. 3) of climatological monthly mean P anomalies (annual mean removed). This seasonal cycle is presented in Fig. 6 for every region. Unit used is millimetre per month per unit area (mm/month). Note that significant gaps in the MSU data set prevented an accurate calculation of P anomalies in polar regions (the NNP and NNA regions) and in December for most regions.

5.1 Pacific ocean

In the northern North Pacific, all data sets agree on a well-marked seasonal cycle, but the amplitude of the cycle varies significantly from one data set to another. Both NWP estimates exhibit a large amplitude seasonal cycle (85 mm/month for ECMWF and 70 mm/month for NCEP). They disagree about the occurrence of maximum/minimum precipitation (December/June in ECMWF and November/July in NCEP). Both data sets agree within 10 mm/month or better on month-to-month value except for December and January (20-mm/month difference). Comparing the two COADS-derived data sets, we find a large difference in the amplitude of the cycle (80 mm/month for UWM and 45 mm/month for SOC) and a shift in the occurrence of the winter maximum (September in SOC and January in UWM) and the summer minimum (May in SOC and July in UWM). The only satellite product available at this latitude (CMAP) shows a seasonal cycle similar to SOC in amplitude (50 mm/month), a summer minimum in May and a winter maximum spread between October and November.

In the western North Pacific, ECMWF, CMAP and SOC show a remarkably similar seasonal cycle (agreement is always better than 5 mm/month), low P occurring in March and April and high P in August. The amplitude of the cycle is nearly 60 mm/month. NCEP cycle appears shifted by 2 or 3 months, low P being observed in May and high P in October and November. UWM differs (sometimes by more than 20 mm/month) from every other data set in summer. The satellite product MSU appears noisy (significant month to month changes) and hardly compares with CMAP.

In the eastern North Pacific, all data sets show a well-marked seasonal cycle of amplitude 40 to 50 mm/month, with a summer minimum in May/June and P maximum in the fall (spread between September to November according to the data set). Agreement on month-to-month values is generally within 10 mm/month except for UWM.

In the equatorial Pacific, satellite and NWP products agree on the occurrence of P minimum in February, whereas COADS-derived products have it in March. All data sets agree on a season of high P spreading from June to October. CMAP and ECMWF exhibit the seasonal signal of largest amplitude (nearly 120 mm/month) and a month-to-month agreement generally better than 10 mm/month. SOC and MSU are similar (both are noisy), and when compared to CMAP and ECMWF, they show higher P anomalies during the season of low precipitation, and comparable P anomalies during the season of high precipitation (except in July). NCEP and UWM exhibit the seasonal signal of the smallest amplitude (55 mm/month). In this region so important for the freshwater budget of the Pacific Ocean, differences between data sets are mostly found in the amplitude (up to 60 mm/month in February) rather than in the phase of the cycle.

In the western South Pacific, place of the SPCZ, the seasonal cycle is qualitatively similar in all data sets, with precipitation reaching a maximum in February/March and a minimum in September/October. This cycle is out of phase with the cycle of the equatorial Pacific region (with a smaller amplitude) due to the southward shift of the ITCZ in the Austral winter, a signal well-captured by all data sets. Discrepancies in the amplitude of the cycle are similar to those noticed in the equatorial Pacific region.

In the eastern South Pacific, a region of low precipitation, the seasonal cycle of P is remarkably similar in phase and amplitude for all data sets except UWM. Agreement is generally better than 5 mm/month, except during the rainy season of March and April for ECMWF. The seasonal cycle in UWM does not seem coherent.

5.2 Atlantic Ocean

The northern North Atlantic shows, for most data sets, a seasonal cycle with high P in December/January and low P in June/July. Discrepancies between data sets are significantly smaller than in NNP. NWP products agree with each other (and with UWM) within less than 10 mm/month. SOC and CMAP look alike and differ from the others by 20 to 40 mm/month. Their P minimum occurs earlier (in May) and the amplitude of the cycle is smaller (55 mm/month compared to 110 mm/month for the others). There is no reliable MSU observation for this latitude.

The western North Atlanticand the eastern North Atlantic are regions where many air–sea observations exist, and we expect NWP analyses to be well-constrained, and the sampling of COADS to be the densest. Good agreement, or at least better than elsewhere, is therefore expected between in situ and model estimates of precipitation. Indeed, agreement is quite good for all data sets,

except for MSU and to a larger degree for UWM. In the WNA, most data sets indicate June as an anomaly of higher P in the middle of the dry season (which lasts from April to July), but its amplitude is smaller in NCEP and UWM. The same kind of anomaly is observed in the ENA with the month of May. Agreement between data sets is generally within 5 to 10 mm/month for a cycle whose amplitude is nearly 60 mm/month in the western North Atlantic (except for UWM and MSU), and within 5 mm/month for a cycle of 50 mm/month amplitude in the eastern North Atlantic (except for UWM).

In the equatorial Atlantic, all data sets agree on the occurrence of the dry season in February/March, and a long rainy season (May to November) with two peaks of precipitation, one in May/June and another of slightly greater amplitude in October/November. This pattern is not so well-reproduced in MSU, which exhibits its maximum in July/August. The amplitude of the seasonal cycle is the largest in ECMWF (110 mm/month) and CMAP (90 mm/month) due to larger peak values. It is of the order of 65 mm/month for the other data sets, which generally agree with each other within 10 mm/month.

In the western South Atlantic, all data sets draw different seasonal cycles. They all agree (within 5 mm/month), however, on the February minimum. But for other individual months, differences are usually as large as 15 mm/month (and can rise up to 35 mm/month) for a seasonal cycle whose amplitude is of the order of 35 to 40 mm/month.

In the eastern South Atlantic, the seasonal cycle of CMAP and NWP products follow each other within 10 mm/month (with a cycle of amplitude of 50 mm/month). COADS-derived products agree with each other within 5 or 10 mm/month, but present a cycle of smaller amplitude (30 mm/month). MSU is again peculiar, close to COADS in fall and to CMAP for the rest of the year.

5.3 Indian Ocean

In the western Indian, the mean seasonal cycle is characterised by two periods of high precipitation in May–July and November–December in every data set. Most data sets agree on the amplitude of the cycle (around 60 mm/month) except the two NWP products (80 mm/month for ECMWF and 100 mm/month for NCEP). COADS-derived products are very similar to each other (agreement better than 5 mm/month for every individual month) and are close to satellite products CMAP and MSU.

In the eastern Indian, agreement between data sets is found only for the first 5 months of the year (January to May), a period that includes the occurrence (in March) of the low P anomalies. For the rest of the year, there is no obvious coherence in the month-to-month variations of the various data sets, which may differ one from each other by 10 to 20 mm/month (and sometimes over 30 mm/month for MSU) for an amplitude of the cycle which is of the order of 50 mm/month or less (for SOC).

In the southern Indian, the seasonal cycle is characterised by a regular decrease of P from its maximum in February to its minimum in September or October. Only UWM shows a significantly different cycle, placing the rainy season between May and July. Despite this qualitative agreement in the phase of the cycle, a large disagreement remains on the amplitude, which varies from 30 to 50 mm/month, according to data sets. MSU and CMAP are almost identical from January to August, but diverge by more than 10 mm/month the rest of the year.

5.4 Southern Ocean

In the Southern Ocean, CMAP and NCEP show a seasonal cycle in good agreement (5 mm/month or better), as expected at high latitudes. Both show regular variations from a dry summer season (November to January) to a rainy period in June and July. However, NCEP cycle has greater highs and smaller lows; thus, its amplitude (30 mm/month) exceeds that of CMAP by 10 mm/month. ECMWF lags by a month and presents a doubtfully low P anomaly in February. Its amplitude is similar to that of NCEP. Both COADS-derived data sets do not reproduce this smooth seasonal cycle, presenting a significant month-to-month noise. MSU is not coherent at these high latitudes.

5.5 Remarks

The agreement between data sets in their representation of the climatological seasonal cycle remains very qualitative and is generally better on the phase than on the amplitude. Considering that the above analysis has been made on quantities integrated over large spatial areas and averaged over 14 years, it is not encouraging to find discrepancies of the order of 20 mm/month (20% or more of the amplitude of the seasonal cycle).

A remarkable agreement is sometimes observed, like between SOC and CMAP in the western Indian, between ECMWF and SOC in the western North Atlantic, or between ECMWF and NCEP in the northern North Atlantic. But these appear as exceptions.

UWM and MSU are the two data sets which differ most often from the others. The best consistency is generally found between the two NWP products and the satellite CMAP product, especially in the regions of low P of the eastern mid-latitude ocean basins (in both hemispheres) and in equatorial regions.

6 Interannual variability

6.1 Observation of peculiar events

Peculiar events have been observed during the 1993–1996 period in the tropical Pacific Ocean using TOPEX or GPCP estimates of P (Quartly et al. 1999). These events are the splitting of the ITCZ in March–April, and the cut of the

SPCZ in July–August. These events are not present every year. In this section, we investigate the splitting of the ITCZ in March 1993.

According to Quartly et al. (1999) and as noticed in TOPEX and GPCP in March–April in 1993–1996, the distribution of precipitation shows two zonal bands, one along 8°N and another (with lower values of *P*) a few degrees South of the equator. These two bands of high precipitation in the eastern Pacific were interpreted as resulting from a temporary split of the ITCZ.

The distribution of *P* in March 1993 is shown for the various data sets in Fig. 7 and is compared to the *P* fields of GPCP and TOPEX.

We first note that in 1993, this two-band pattern is better marked in GPCP than in TOPEX. It is most marked in the satellite products CMAP, MSU and HOAPS. There is no clear split in any of the COADS-derived data sets (no figure shown for SOC), and we cannot say if it is because of an under-sampling or because of the interpolation procedure. It is reproduced by NWP models, although ECMWF does not show a clear separation of the bands of high *P* as shown in satellite products, and NCEP shows a very wide southern band. The same pattern occurred again in March 1994 in all data sets which had it in 1993 (no figure shown), again well seen in satellite estimates but with different intensity.

Concerning the cutting of the SPCZ, according to the study of Quartly et al. (1999) with the GPCP data set, it was observed to occur in July–August 1993 at about 225°E-30°S, resulting in a second *P* maximum centred at 250°E-30°S. This pattern is relatively well-seen in August 1993 in every satellite-based *P* estimate and is also reproduced by NWP models (no figure shown). COADS-derived products do not reproduce this event, showing a limitation to reproduce regional events at the interannual time scale.

6.2 Low-frequency variability

In this section, we proceed to a comparison of the low-frequency variability of the *P* estimates provided by the six data sets covering the common 14-year period 1980–1993.

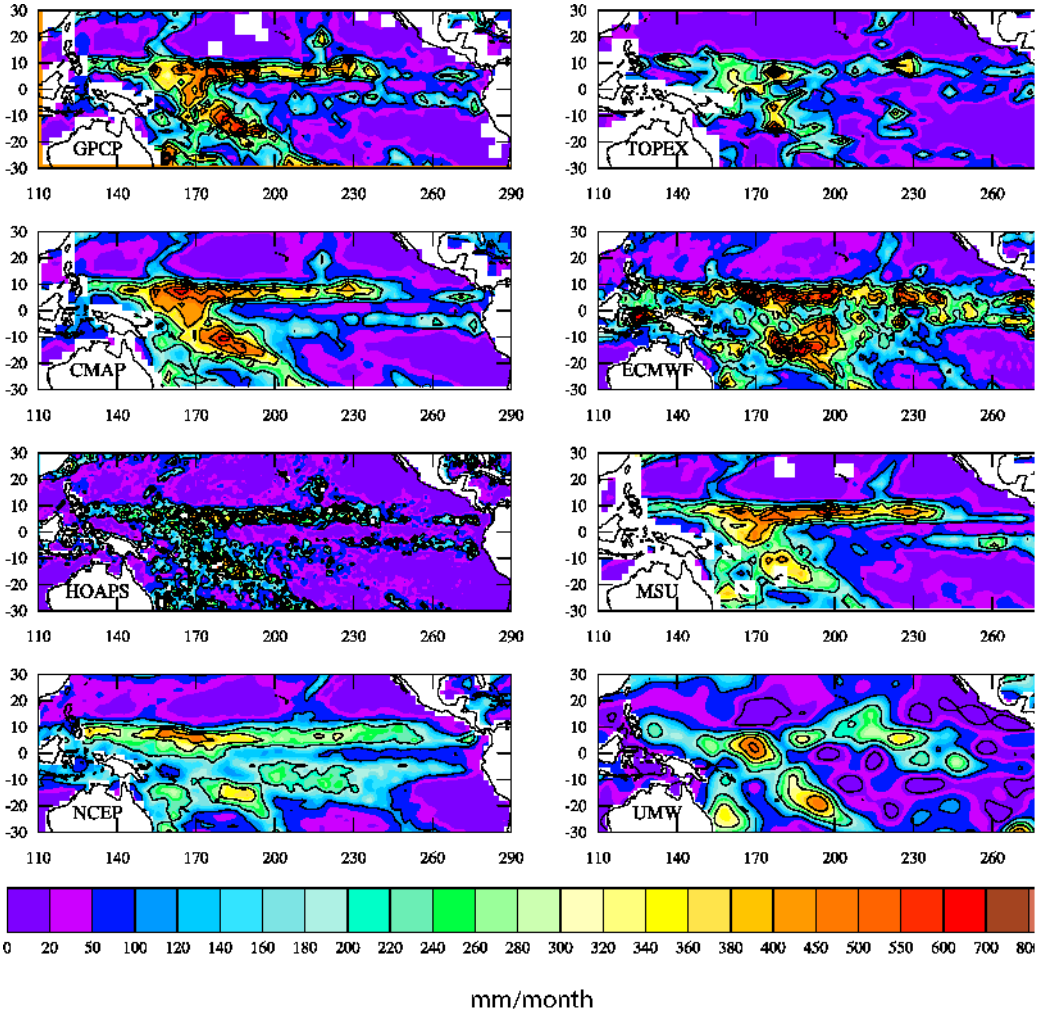

Fig. 7 Monthly precipitation over the equatorial Pacific Ocean in March 1993 for eight data sets. The *colour bar* ranges from 0 to 900 mm/month with irregular spacing. Contour intervals in *dark lines* range from 0 to 800 mm/month with a regular spacing of 100 mm/month

Low-frequency anomalies of P over the 16 areas defined in Fig. 3 are obtained as follows: The climatological mean is subtracted from the 14-year long monthly mean time series, and a 12-month running average is performed, followed by single Hanning filter. The resulting time series are shown in Fig. 8. Due to the smoothing applied, series

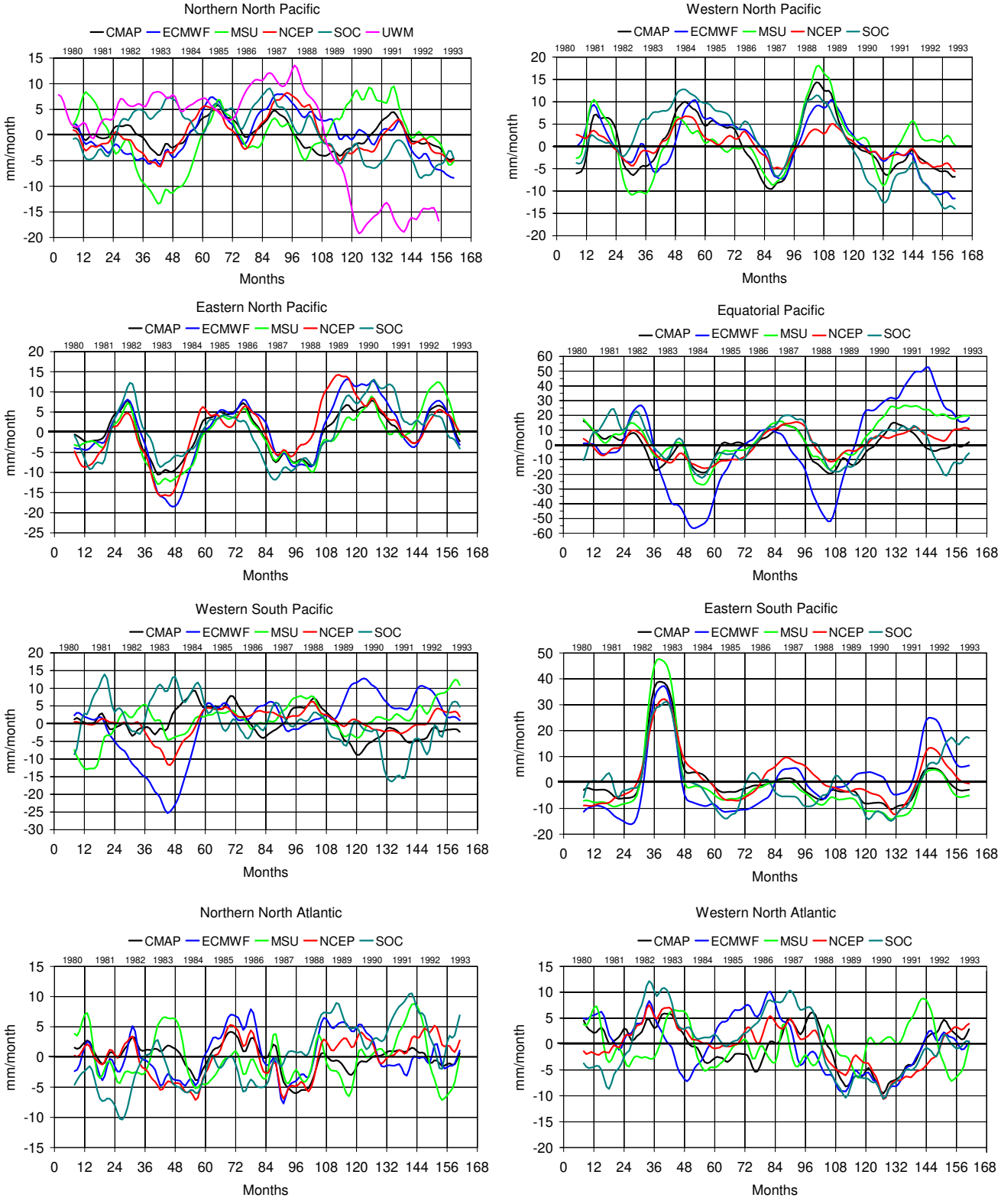

Fig. 8 Monthly mean time series of low frequency precipitation anomalies over the period 1980–1993 for the 16 ocean regions defined in Fig. 3, for the six data sets having the period 1980–1993 in common

Fig. 8 (continued)

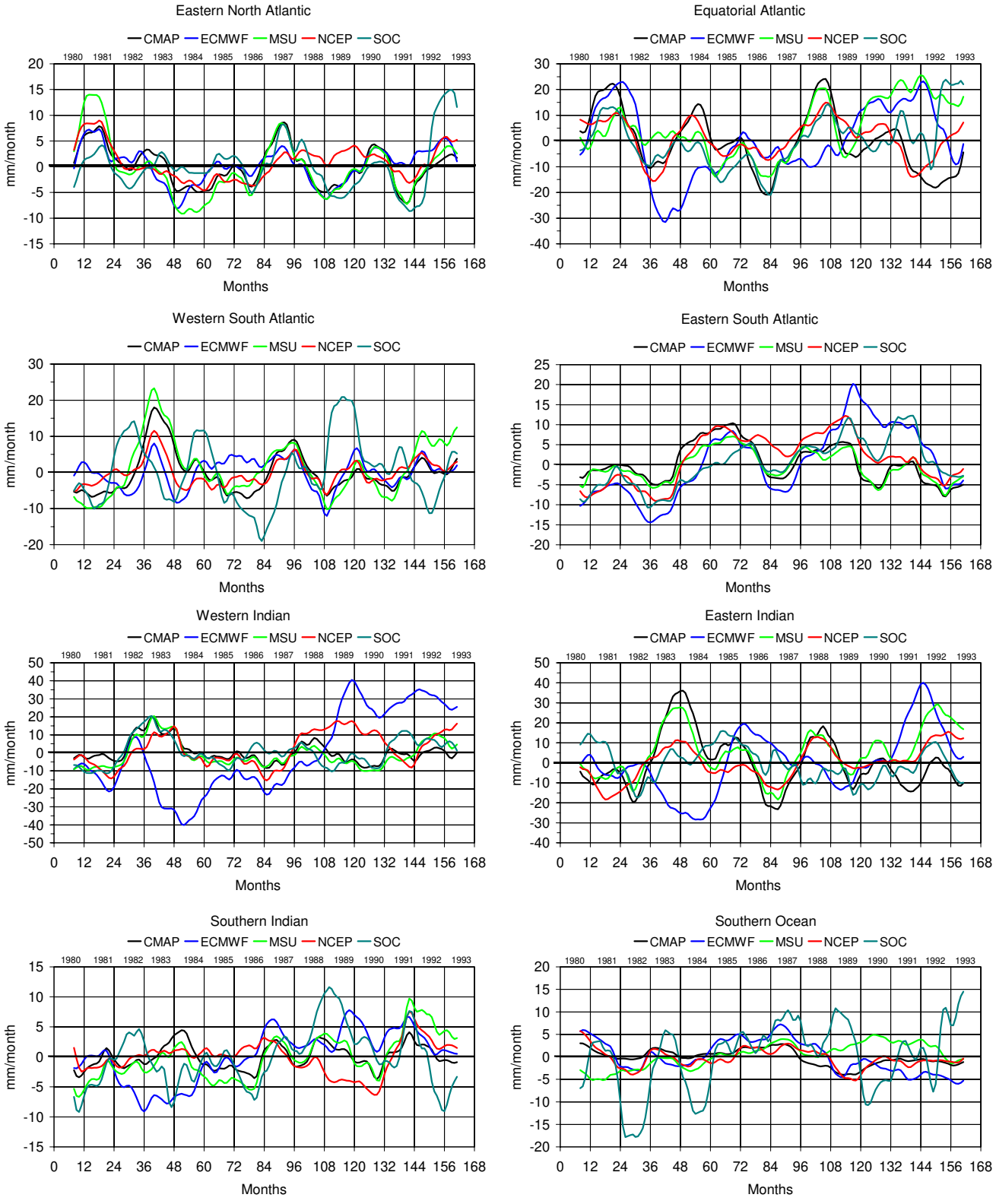

are not complete in 1980 and 1993. Note that the correlation coefficients between all series are shown for all regions in Table 3. In the following, we consider that two series are well-correlated when the correlation coefficient is above the 99% significance level and the variance explained by this correlation is above 50% (i.e. correlation coefficient above 0.7).

UWM, whose record begins in 1945, suffers from two different processing algorithms before and after 1989. Starting in 1989, monthly mean anomalies have been calculated from the mean of 1945–1989 and not for the whole data record. The effect of this is a shift of the series in 1989, as shown in the first plot of Fig. 8 (for the NNP region). It is therefore meaningless to investigate the interannual variability of this data set, which will not be shown in the other regions in Fig. 8. It will not be discussed any longer in this section. It is clear that it should not be used for any purpose related to interannual variability.

6.2.1 Pacific Ocean

In the western North Pacific, the phase of the low-frequency *P* anomalies compares rather well among data sets. Occurrences of periods of positive anomalies in 1981, 1984–1986 and 1988–1989, and of negative anomalies in 1982–1983, 1986–1987 and 1990–1993 are shared by all data sets. Correlation coefficients between series (Table 3) are generally high (i.e. above the critical value of 0.7). The highest correlation is obtained between the two NWP products ECMWF and NCEP (0.88), and the lowest between MSU and SOC (0.38) and MSU and ECMWF (0.57). Note, however, that MSU is well-correlated with the

Table 3 Correlation coefficients between the low frequency anomalies of CMAP, ECMWF, MSU, NCEP and SOC over the period 1980–1993

	CMAP	ECMWF	MSU	NCEP	SOC
	Northern North Pacific NNP				
CMAP		0.59	0.41	0.65	0.36
ECMWF	0.81		0.42	0.85	0.39
MSU	0.81	0.57		0.21	-0.45
NCEP	0.83	0.88	0.62		0.39
SOC	0.75	0.75	0.38	0.79	
	Western North Pacific WNP				

	CMAP	ECMWF	MSU	NCEP	SOC
	Eastern North Pacific ENP				
CMAP		0.94	0.91	0.82	0.80
ECMWF	0.59		0.86	0.88	0.77
MSU	0.77	0.89		0.70	0.71
NCEP	0.68	0.72	0.83		0.64
SOC	0.73	0.43	0.53	0.60	
	Equatorial Pacific EP				

	CMAP	ECMWF	MSU	NCEP	SOC
	Western South Pacific WSP				
CMAP		-0.30	0.09	0.19	0.40
ECMWF	0.75		0.08	0.66	-0.53
MSU	0.99	0.76		0.37	-0.16
NCEP	0.91	0.83	0.91		-0.16
SOC	0.81	0.70	0.81	0.75	
	Eastern South Pacific ESP				

The 99% significance level estimated through the z-Fisher transform (von Storch and Zwiers 1999) is 0.21

Table 3 (continued)

	CMAP	ECMWF	MSU	NCEP	SOC
	Northern North Atlantic				
CMAP		0.44	0.48	0.52	-0.10
ECMWF	0.48		-0.10	0.77	0.21
MSU	0.11	-0.08		0.05	0.29
NCEP	0.75	0.62	-0.21		0.29
SOC	0.66	0.57	-0.09	0.88	
	Western North Atlantic WNA				

	CMAP	ECMWF	MSU	NCEP	SOC
	Eastern North Atlantic ENA				
CMAP		0.72	0.93	0.64	0.56
ECMWF	0.10		0.81	0.55	0.41
MSU	0.16	0.48		0.80	0.49
NCEP	0.76	0.12	0.11		0.41
SOC	0.35	0.29	0.64	0.51	
	Equatorial Atlantic EA				

	CMAP	ECMWF	MSU	NCEP	SOC
	Western South Atlantic WSA				
CMAP		0.29	0.90	0.79	0.05
ECMWF	0.37		0.35	0.48	-0.21
MSU	0.95	0.45		0.79	-0.04
NCEP	0.73	0.70	0.79		0.11
SOC	0.33	0.88	0.48	0.68	
	Eastern South Atlantic				

Table 3 (continued)

	CMAP	ECMWF	MSU	NCEP	SOC
	Western Indian WI				
CMAP		-0.23	0.87	0.34	0.65
ECMWF	-0.51		-0.05	0.45	0.12
MSU	0.68	0.03		0.42	0.78
NCEP	0.54	0.05	0.88		0.15
SOC	0.23	0.08	0.08	-0.13	
	Eastern Indian EI				

	CMAP	ECMWF	MSU	NCEP	SOC
	South Indian SI				
CMAP		0.13	0.77	0.36	0.37
ECMWF	0.68		0.41	-0.04	0.33
MSU	-0.21	-0.11		0.44	0.39
NCEP	0.75	0.70	-0.09		-0.22
SOC	0.00	0.17	0.29	0.27	
	Southern Ocean SO				

other satellite product CMAP. The amplitudes of the peaks and troughs of the anomalies vary significantly (5 to 10 mm/month) from one data set to another, but no systematic difference is observed according to the origin of the data. For example, the positive *P* anomaly of 1983–1985 is the largest in SOC, it is comparable in CMAP and ECMWF, and it is the smallest in NCEP and MSU. In the following period of positive anomalies in 1988–1989, the two satellite products are above all the others, SOC and ECMWF are similar, and NCEP is again the smallest. In general, inter-annual variations are of the order of 15 to 25 mm/month (from peak to trough) to be compared to a climatological annual mean of the order of 110 mm/month (or 1,300 mm/year, Fig. 5).

Other regions of the Pacific where the low-frequency variability of *P* appears to be in agreement between data sets are the eastern North Pacific, the equatorial Pacific and the eastern South Pacific. In these regions, and as already noticed in the western North Pacific, the various data sets agree roughly about the occurrence of the periods of high and low *P*, generally in a tight relation with the occurrence of El Nino (1982–1983, 1986–1987 and 1991–1992) and La Nina (1983, 1988–1989) events. Correlation coefficients obtained from the time series of *P* anomalies are high and comparable to those obtained in the western North Pacific, best correlation being noticed in the eastern North Pacific. However, each region has peculiarities, so conclusions drawn for one region often do not hold for another.

In the equatorial Pacific for example, the amplitude of inter-annual variations of *P* is of the order of 20 mm/month. ECMWF exhibits variations, which are three times those of the other data sets. Therefore, the good agreement noticed in the western North Pacific between the two reanalysis products and the CMAP satellite product does not hold for this region, which is characterised by a good agreement in phase and amplitude (often within 5 mm/month) between the NWP products and the MSU product (correlation coefficient above 0.80).

The northern North Pacific and the *western South Pacific* are regions where the correlation coefficients obtained from the time series of *P* anomalies are low, especially in the western South Pacific (Table 3). For the northern North Pacific, the best agreement is found between NWP (0.85). In the western South Pacific, no significant phase agreement is noticed between any series, even between data sets having the same source (no

correlation coefficient above 0.7 for that region in Table 3). It is striking to note how the two satellite products are different. SOC and ECMWF are generally out of phase (correlation coefficient is −0.53). The best phase agreement is found between ECMWF and NCEP (correlation coefficient of 0.66). All data sets agree on the amplitude of the interannual variations, which ranges between 5 and 10 mm/month, except for ECMWF, for which anomalies are once again three times greater.

6.2.2 Atlantic Ocean

Correlation coefficients between time series anomalies are smaller in the Atlantic than in the Pacific, indicating a lesser agreement between data sets.

The western North Atlantic is a good example of the kind of agreement and disagreement that can be observed. A first glance at the low-frequency anomalies of *P* in this region suggests a rough agreement between data sets about periods of *P* excess in 1982–1983, 1985–1988 and 1991–1993, and periods of *P* deficit in 1984–1985 and 1989–1991. A closer analysis shows that the agreement between the various time series is highly variable according to the period considered. The period of negative precipitation anomalies of 1989–1991 is seen in all data sets (except MSU), which agree within a few millimetre per month. They describe a sharp decrease of precipitation in 1988, which leads to a deficit in precipitation of nearly 10 mm/month in 1989 and 1990, followed by an increase in 1991, with year 1992 showing a small excess in *P* (5 mm/month). On the contrary, differences between data sets are numerous during the 5-year period 1983–1987. ECMWF shows a strong decrease of precipitation in 1983 (from +7 to −7 mm/month). A similar decrease is seen in the other data sets, shifted by half a year in MSU and by a year in CMAP, SOC and NCEP. The period of low *P*, which follows this decrease, is also differently represented by the various data sets. It barely lasts a year in ECMWF, whose anomalies turn positive again at the end of 1984, but lasts for 2 years (1984–1985) in NCEP and SOC and almost 3 years (1984–1986) in CMAP.

Again, it was not possible to extract a typical behaviour of the low-frequency variability according to the source of the data. Indeed, the data sets that appear the most in agreement with each other over the whole 14-year period in this area are SOC and NCEP (correlation coefficient is 0.88).

In the equatorial Atlantic, the only data sets that appear coherent for the whole period are CMAP and NCEP. Both are basically in phase, and their differences mainly lie in the amplitude of the anomalies, which are greater (often double) in CMAP. The correlation coefficient of the two series is 0.76. As shown in Table 3, correlations between the time series of *P* anomalies for this region are pretty low, despite a correlation of 0.64 between SOC and MSU. As it appears in Fig. 8, if the various data sets are able to agree on a few specific events of excess or deficit in precipitation, they do not do so over the whole record. ECMWF for example is catching the *P* excess of 1981–1982 and the *P* deficit of 1983 (although it clearly overestimates its amplitude), but is missing the excess in *P* of 1988, which every other data set exhibits. A striking example of disagreement between data sets from the same origin is given in 1991–1992, a period when a satellite product (MSU) and a re-analysis product (ECMWF) both suggest an excess in *P* (over 20 mm/month), whereas another satellite product (CMAP) with another re-analysis product (NCEP) show a deficit (of 15 to 20 mm/month).

The eastern South Atlantic, at the eastern side of a mid-latitude ocean basin, is characterised by a strong atmospheric subsidence and low precipitation (25 to 35 mm/month in annual mean depending on the data set—see Fig. 5). Therefore, as shown in Fig. 8, the amplitude of the low-frequency variations (5 to 10 mm/month) can reach a significant fraction of the mean. Despite large differences in long-term trends (small and negative in the satellite products, large and positive in the other products), there is a good agreement in the phase between all data sets. Agreement between the two satellite products CMAP and MSU is remarkable in the phase (correlation is very high, 0.95) but also in amplitude (except for a 2-year period in 1984–1985). All data sets agree about the periods of precipitation deficit between 1980 and 1983, in 1987 and between 1992 and 1993. They also agree about two periods of excess precipitation between 1984 and 1986, and between 1988 and 1989. Note that NCEP merges these two periods in a single long one of 7 years of *P* excess. As for all regions, which show a reasonable agreement in the phase, significant differences (5 mm/month or more) are often found in the amplitude of the anomalies. Among all data sets, ECMWF is again the one that shows the largest anomalies.

6.2.3 Indian and Southern Oceans

In the Indian Ocean, discrepancies between data sets are large. The two satellite products CMAP and MSU are the only ones to be in agreement with each other and well-correlated over the whole period (Table 3). In the western and the eastern Indian, NCEP is comparable to the satellite products between 1980 and 1988 but is very different later on. It is different in the southern Indian, where agreement is null before 1987 and is rather good in phase but not in amplitude (too large) after that date. SOC low-frequency variability follows the satellite products in the western Indian (correlation of 0.65 with CMAP and 0.78 with MSU) but is very different from all the other data sets in the eastern Indian and the south Indian. ECMWF low-frequency anomalies do not show similarities with any other data set, with fairly small (when not negative) correlation with other data sets (Table 3), and amplitudes of 40 mm/month when the other data sets have amplitudes of 20 mm/month.

In the Southern Ocean, a good agreement is found between CMAP and NCEP (as expected at high latitudes

by construction of CMAP), but also between these data sets and ECMWF. All suggest small-amplitude, low-frequency variations (3 to 5 mm/month, although higher in ECMWF), with a period of excess precipitation between 1984 and 1987, and a longer period of deficit between 1988 and 1993. SOC is not coherent with the other data sets (see Table 3), being dominated by large changes of 10 to 20 mm/month from year to year. MSU does not have enough data at high latitudes to be compared.

7 Satellite products HOAPS and GPCP

Because the HOAPS and GPCP data sets do not cover the common 1980–1993 period, they were not included in the above comparison. Nevertheless, these data sets have a significant period in common with CMAP (see Table 2): 7 years for HOAPS (from 1992 to 1998) and 8 years for GPCP (1988 to 1995). In this section, we compare these two satellite products with the merged CMAP product over their respective common periods.

7.1 Regional budgets

The spatial patterns of precipitation of these data sets have been described and compared to all the other *P* fields in Section 3. The focus of this section is on regional budgets of the mean precipitation.

Figure 9 shows the average mean precipitation over each of the 16 ocean regions defined in Fig. 3, for GPCP and CMAP (mean for 1988 to 1995) and for HOAPS and CMAP (mean for 1992 to 1998). The 14-year mean of CMAP (1980–1993), which was compared to the other *P* estimates in the previous sections, is also reported.

The first remark is that CMAP varies very little (by just a few percent) from one period to another in all regions, with two exceptions, where changes are 10% or more. The first one is the eastern South Pacific, where CMAP shows for the period 1980–1993 a mean value of *P*, which is 51 mm/year greater than in 1988–1995. As this region is characterised by low *P*, this represents a relative increase of 19%. This is easily explained by the greater number of El Nino events included in the 1980–1993 period, these events having an impact on the precipitation budget of this region of usually low *P*. The second is the western Indian, where CMAP shows for the period 1980–1993 a mean value of *P*, which is 94 mm/year (10%) smaller than in 1992–1998. Therefore, it seems reasonable to consider that the results drawn from the previous sections, where the six data sets covering the 1980–1993 period have been compared, can be extended and used in the present comparison between CMAP, HOAPS and GPCP.

GPCP and CMAP are very comparable, and the mean *P* values they propose agree within 10% or better in most regions. The largest disagreement is found in the two regions that show *P* values of the order of 2,000 mm/year or higher.

In the eastern Indian, GPCP proposes a mean *P* value which is 15% smaller than the one proposed by CMAP for the same period. Note that in this region, CMAP values are the highest among all climatologies (see Fig. 5), and GPCP appears, with nearly 2,000 mm/year, to lie between the NWP products that are above this value and the COADS-derived products that are close to 1,800 mm/year.

In the equatorial Pacific, GPCP is smaller by 10% than CMAP. With again nearly 2,000 mm/year, it compares very well with SOC, MSU and NCEP (Fig. 5).

The only regions where GPCP significantly exceeds CMAP (by nearly 10%) are the western mid-latitude ocean

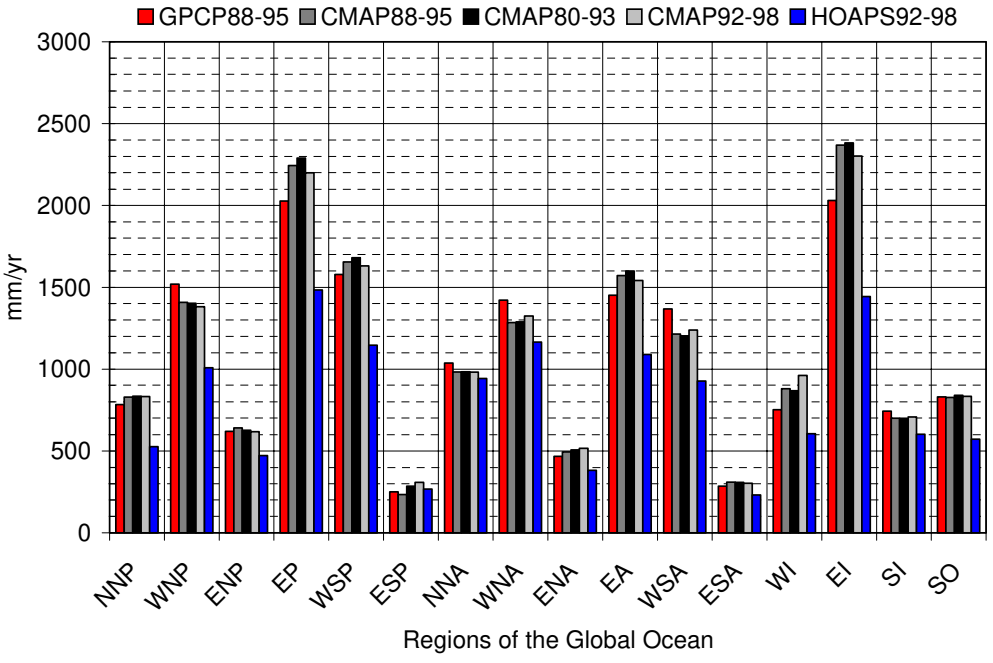

Fig. 9 Spatial average of the mean precipitation (in millimetre per year) for every ocean region defined in Fig. 3, for the CMAP, GPCP and HOAPS data sets. For the purpose of comparison, mean precipitation is calculated for the period 1988–1995 for GPCP (*red*) and CMAP (*dark grey*), for the period 1992–1998 for HOAPS (*blue*) and CMAP (*light grey*). The value obtained for CMAP averaged over the 1980–1993 is shown in *black*

basins (WNP, WNA and WSA), where air–sea interactions are greatly influenced by warm poleward western boundary currents (the Kuroshio Current in the WNP, the Gulf Stream in the WNA and the Brazil Current in the WSA). Thus, GPCP is the data set, which proposes the highest precipitation with MSU and CMAP in these regions (see also Fig. 5).

In every other region, comments made about CMAP in Section 4 hold for GPCP, the two data sets being very similar.

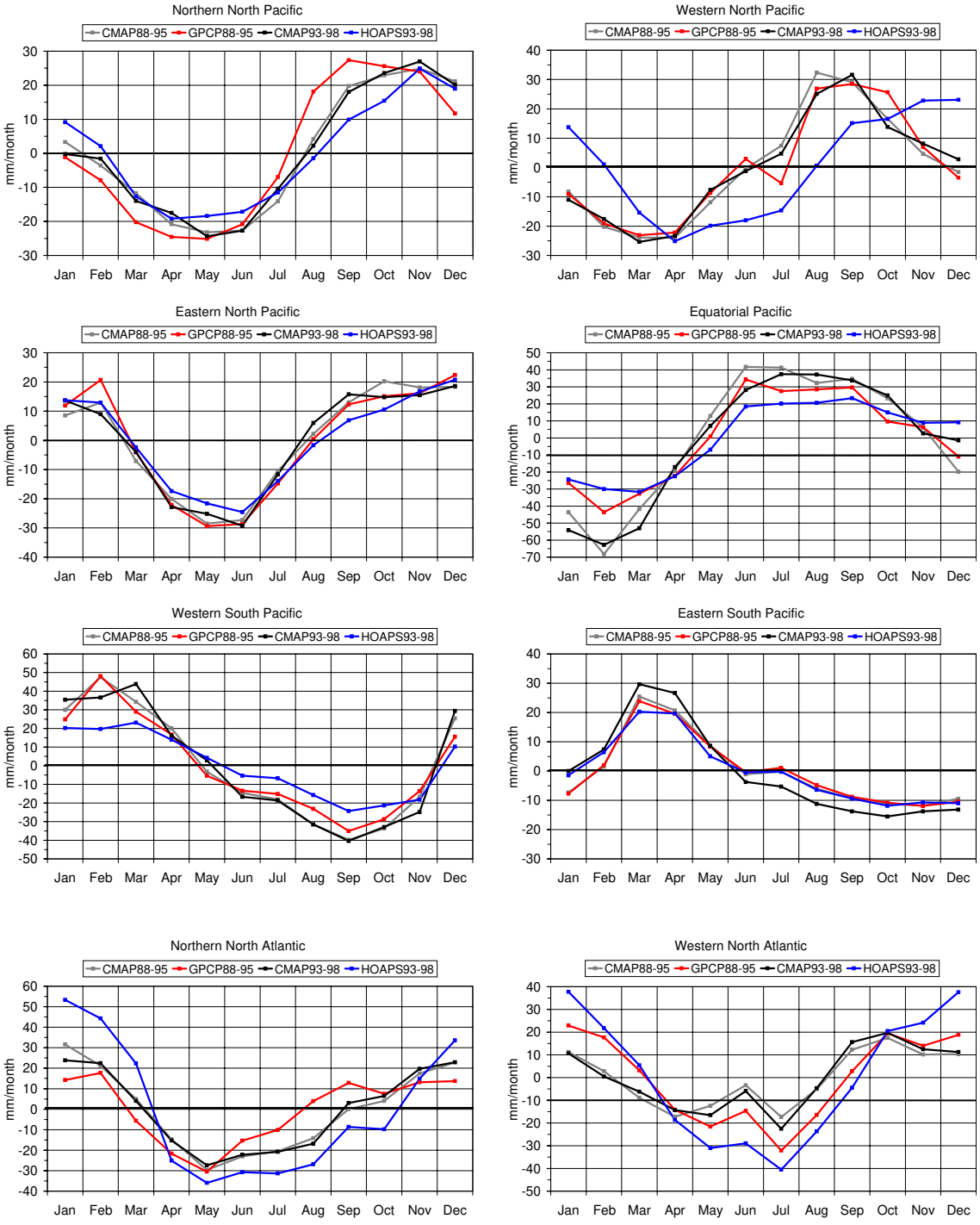

Fig. 10 Climatological seasonal cycle of precipitation (i.e. monthly mean precipitation anomalies) for the 16 ocean regions defined in Fig. 3, for the CMAP, GPCP and HOAPS data sets. Time means used to calculate this cycle (following the same method as for Fig. 6) were performed over periods common to these data sets to make direct comparisons relevant. The seasonal cycles of GPCP (*red*) and CMAP (*grey*) are relative to 1988–1995 and that of HOAPS (*blue*) and CMAP (*black*) to 1992–1998

Fig. 10 (continued)

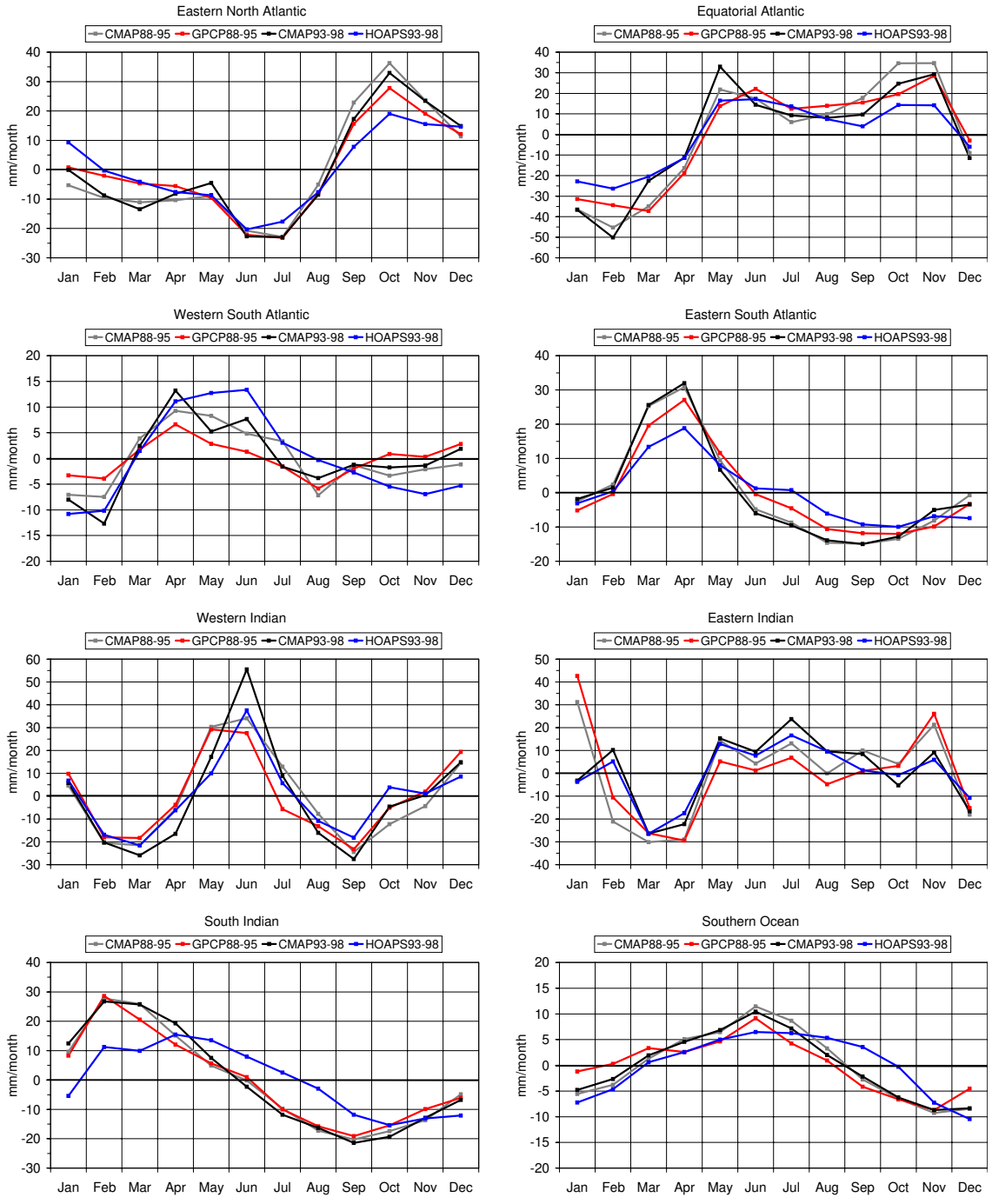

HOAPS shows precipitation values that are systematically and significantly smaller than CMAP and GPCP in every region (30% in average over all regions). Underestimation is especially large in tropical regions (by 800 mm/year in the eastern Indian, 700 mm/year in the equatorial Pacific, 500 mm/year in the equatorial Atlantic and the western South Pacific). HOAPS *P* estimate is comparable to other estimates only in the northern North Atlantic and in the region of low *P* of the eastern South Pacific and South Atlantic. This suggests a systematic bias towards low values (i.e. underestimation) in this data set.

7.2 Seasonal variability

The climatological seasonal cycle of precipitation (i.e. monthly mean precipitation anomalies) is shown in Fig. 10 for the 16 ocean regions. The seasonal cycle of GPCP has

been calculated relative to the period 1988–1995 and that of HOAPS for 1992–1998. The seasonal cycle of CMAP for these two periods is reported for comparison.

GPCP cycle follows the cycle of CMAP in almost every region. The northern North Pacific, where CMAP is largely influenced by NCEP values, is the region where HOAPS differs most (over the same period). It shows a cycle slightly shifted, extremes occurring earlier in the year. In the equatorial Pacific, the February minimum is smaller by 30 mm/month in GPCP, and a difference of nearly 10 mm/month is found in July and October. Elsewhere, both data sets agree within a few millimetre per month and always better than 5 mm/month. Considering the generally poor agreement noticed between data sets, we could qualify such agreement as very good and this is likely due to the important weight of satellite observations in both data sets.

HOAPS cycle is in phase with CMAP in most regions with a few exceptions. In the western North Pacific, the spring minimum is delayed by a month (from March to April) and so is the shift from the dry season to the wet season by 2 months (June in CMAP and August in HOAPS). In the western South Atlantic, the *P* maximum of the wet season is shifted from April to June. The southern Indian and the Southern Ocean are also regions where the phase of the seasonal cycle is different in HOAPS and CMAP. The amplitude of the seasonal cycle is generally smaller in HOAPS than in any other data set, especially in regions of high precipitation, like the equatorial Pacific (50 mm/month compared to 100 mm/month for CMAP), the western South Pacific or the equatorial Atlantic. The seasonal cycle is also smaller in HOAPS in the regions of subsidence, like the eastern South Pacific and the eastern South Atlantic (not shown). This is consistent with the systematic underestimation of precipitation already noticed for the mean.

7.3 Interannual variability

In this section, we proceed to a comparison of the low-frequency variability of the *P* estimates provided by the HOAPS and GPCP data sets. Figure 11 shows monthly mean time series of low-frequency precipitation anomalies between 1988 and 1998 for the regions defined in Fig. 3. For the period 1988–1995, CMAP and GPCP anomalies are calculated with regard to the 1988–1995 mean. For the period 1992–1998, CMAP and HOAPS anomalies are calculated with regard to the 1992–1998 mean. This explains the offset between the two sets of curve for CMAP. The filtering applied is the same as the one described in Section 6.2. Correlations between the GPCP and CMAP low-frequency time series over their respective periods of comparison are shown in Table 4. Correlation coefficients above 0.3 are above the 99% significance level. In the following, we shall consider that two series are well-correlated when the variance explained by this correlation is above 50% (i.e. coefficient above 0.7).

7.3.1 GPCP low-frequency variability

Interannual variations of the GPCP data set agree rather well with that of CMAP for the same period (1988–1995). Correlation between both series is rather high (0.82 in average for 14 of the 16 ocean regions), and only two regions show insignificant correlation (less than 0.26) (Table 4).

The western South Pacific (Fig. 11) is the region where the agreement between these two time series is the poorest, both signals appearing often out of phase (correlation of 0.11). A poor agreement was already noticed in this region between all *P* estimates in Section 6.2.1, where very small or negative correlation where found (Fig. 8, Table 3). It is clear that the determination of rainfall in this area, dominated by the SPCZ, is particularly difficult by all means.

The Southern Ocean is another region of strong discrepancies between the two data sets (correlation coefficient of 0.26). A strong disagreement was already noticed over the 1980–1993 period between the six data sets compared in Section 6 (small or negative correlation, Table 3), except for CMAP and NCEP, the first being known to be strongly constrained by the latter.

In the other ocean regions, the agreement between GPCP and CMAP low-frequency variability is rather good. Wet and dry periods occur at the same time in both series, although amplitudes may be different. Correlation is generally greater than 0.8 and is remarkably good (0.98) in the eastern South Pacific (Fig. 11, the interannual variability of *P* is characterised by a peak of high *P* in early 1992 associated with the 1991 El Nino) and the eastern South Atlantic. In the equatorial Pacific, the 1991 El Nino is characterised in both data sets by a peak of high precipitation (but with a greater amplitude in CMAP, correlation of 0.80 between both series).

When correlation is below 0.8, like in the northern North Pacific (correlation of 0.71) or the northern North Atlantic (correlation of 0.61), it is because of a disagreement about a peculiar event. In the northern North Pacific for example, the difference between the series occurs in 1993, a year given as wet in GPCP and as dry in CMAP. In the eastern Indian (no figure shown) both series show a very comparable deficit in *P* during the 1991 El Nino (correlation of 0.7). Overall, the agreement of CMAP with GPCP is significantly better than what was noticed with all the other data sets among which it has been compared to in this study.

7.3.2 HOAPS low-frequency variability

Interannual variations in HOAPS are also in very good agreement with that of CMAP for the period 1992–1998. Correlation between the two series for the 16 ocean regions is better in average than for GPCP (Table 4) as a result of a very similar representation of the various wet and dry periods (Fig. 11). However, the amplitude

of the low-frequency anomalies of P is significantly smaller in HOAPS. In the regions strongly marked by the 1997 El Nino, for example, the amplitude of the anomalies associated with this event are smaller by 10 mm/month (equatorial Pacific, eastern South Pacific) to almost 20 mm/month (eastern Indian). This is consistent with a systematic underestimation of precipitation in the HOAPS data set, already noticed on the mean budgets and the seasonal cycle. Exceptions are the northern North Pacific, where the amplitude of the wet period in 1994 is twice larger in HOAPS, and the northern North Atlantic (no figure shown), where HOAPS shows in 1993–1994 a wet period of amplitude greater than 10 mm/month whereas it is below 5 mm/month in CMAP. At these northern latitudes, the fact that NCEP, rather than satellite products, largely influences CMAP may explain this difference.

The western South Pacific is again an area where differences between HOAPS and CMAP are important, as it is between all the data sets considered in this study.

Overall, the low-frequency variability described by the satellite product HOAPS agrees very well with that of the merged product CMAP.

8 Conclusion

The freshwater input in the ocean has such an important impact on the salinity and the density flux at the ocean surface that high-quality precipitation estimates at global scale are needed to undertake almost any realistic ocean circulation studies. However, assessing precipitation over the sea remains a difficult task. This paper intends to contribute to this assessment and has carried out a comparison between several data sets, which are available for use in forcing OGCMs. Rather than focusing on a detailed comparison of every P patterns, the paper concentrates on the P budget (i.e. area average) of large areas relevant to ocean dynamics, like mid-latitude gyres or the equatorial waveguide. The objective is to document differences and similarities to provide information useful in selecting a P field as a component of the freshwater forcing of an OGCM, so we have not undertaken to explain the reasons for the discrepancies which were found. Therefore, this analysis should complement other studies that investigated precipitation over oceans in two ways. First, the comparison is made here over at least a decade between the ten major data sets estimated from all available sources, whereas most studies are limited to just a few data sets or over periods of a few months. Second, the point of view is from the ocean side, with a focus on the precipitation budget over regions relevant to the ocean circulation.

Ten data sets from several sources were gathered from: NWP models (ECMWF and NCEP); in situ data (CCR, SOC and UWM); satellite data (MSU, TOPEX and HOAPS) and composite (i.e. combination of satellite, rain gauge or model) data (GPCP and CMAP). The data sets were compared over 16 relatively large regions, representative of large-scale ocean circulation features, to diagnose biases, trends and behaviours linked to their data source. In general, the results of our analysis are not encouraging because most data sets greatly disagree in many regions. Moreover, no systematic differences between the various data sets according to their source were objectively identified on mean, or seasonal or interannual diagnostics, although agreement subjectively appears to be better between data sets of the same source.

A quantitative approach showed that P budgets over the 1980–1993 period are not homogeneously represented among the various climatologies. More precisely, mean P budgets, which represent the average of P over ocean basins and for relatively long time periods, could differ significantly (by several tens of percent in some cases). Such differences after such space–time integration are still very large because they represent several hundred of millimetre per year and would induce over a long period a drift in the salinity of an ocean gyre.

Concerning the seasonal variability of the monthly climatologies (monthly means over the common period), a better agreement was found in phase than in amplitude except in few geographical regions. Differences in amplitude reached 20 to 30% in regions of moderate P and 50 to 60% in regions of high P during the rainy season. Different behaviours, like a shift of the occurrence of the P maximum/minimum, were not found to be characteristic of a source of data; almost every data set has been found, at least in one of the 16 regions studied, to be not in agreement with the others in its description of the seasonal cycle.

Comparison of low-frequency (interannual) variability also pointed out important differences between data sets. Again, discrepancies are more important on the amplitude

Table 4 Correlation coefficients of the low frequency anomalies of precipitation between CMAP and GPCP over the period 1988–1995 (99% significance level of 0.28), and between CMAP and HOAPS over the period 1992–1998 (99% significance level of 0.30)

	GPCP-CMAP 1988–1995	HOAPS-CMAP 1992–1998
NNP	0.71	0.66
WNP	0.89	0.82
ENP	0.79	0.95
EP	0.80	0.93
WSP	0.11	0.57
ESP	0.98	0.99
NNA	0.61	0.79
WNA	0.93	0.36
ENA	0.88	0.86
EA	0.95	0.94
WSA	0.79	0.34
ESA	0.98	0.94
WI	0.91	0.97
EI	0.70	0.94
SI	0.65	0.60
SO	0.26	0.55

Significance levels are defined according to the z-Fisher transform (von Storch and Zwiers 1999)

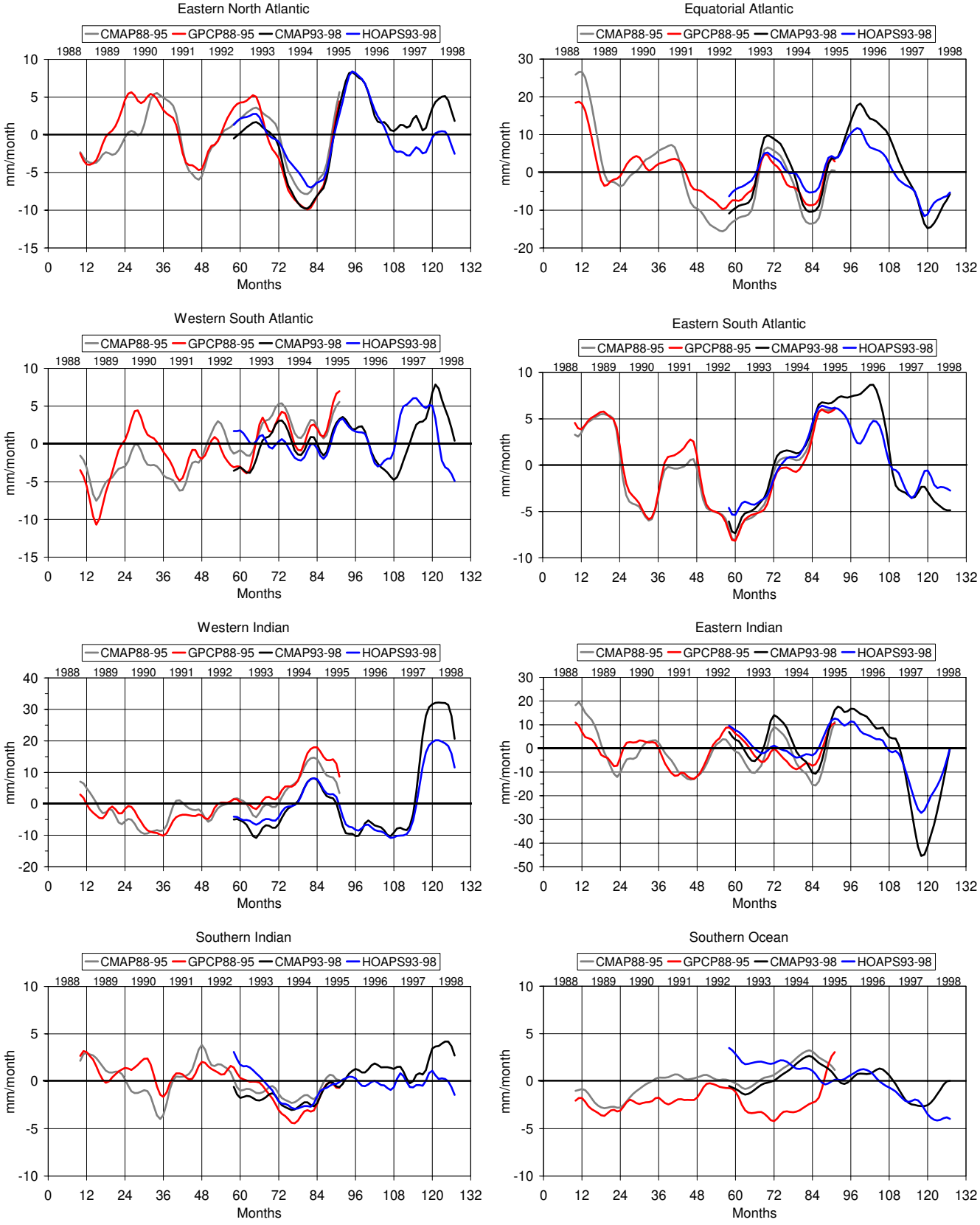

Fig. 11 Monthly mean time series of low frequency precipitation anomalies between 1988 and 1998 for the 16 ocean regions defined in Fig. 3, for the GPCP, HOAPS and CMAP data sets. For the period 1988–1995, CMAP (*grey*) and GPCP (*red*) anomalies are calculated with regard to the 1988–1995 mean. For the period 1992–1998, CMAP (*black*) and HOAPS (*blue*) anomalies are calculated with regard to the 1992–1998 mean. This explains the offset between the two sets of curve

Fig. 11 (continued)

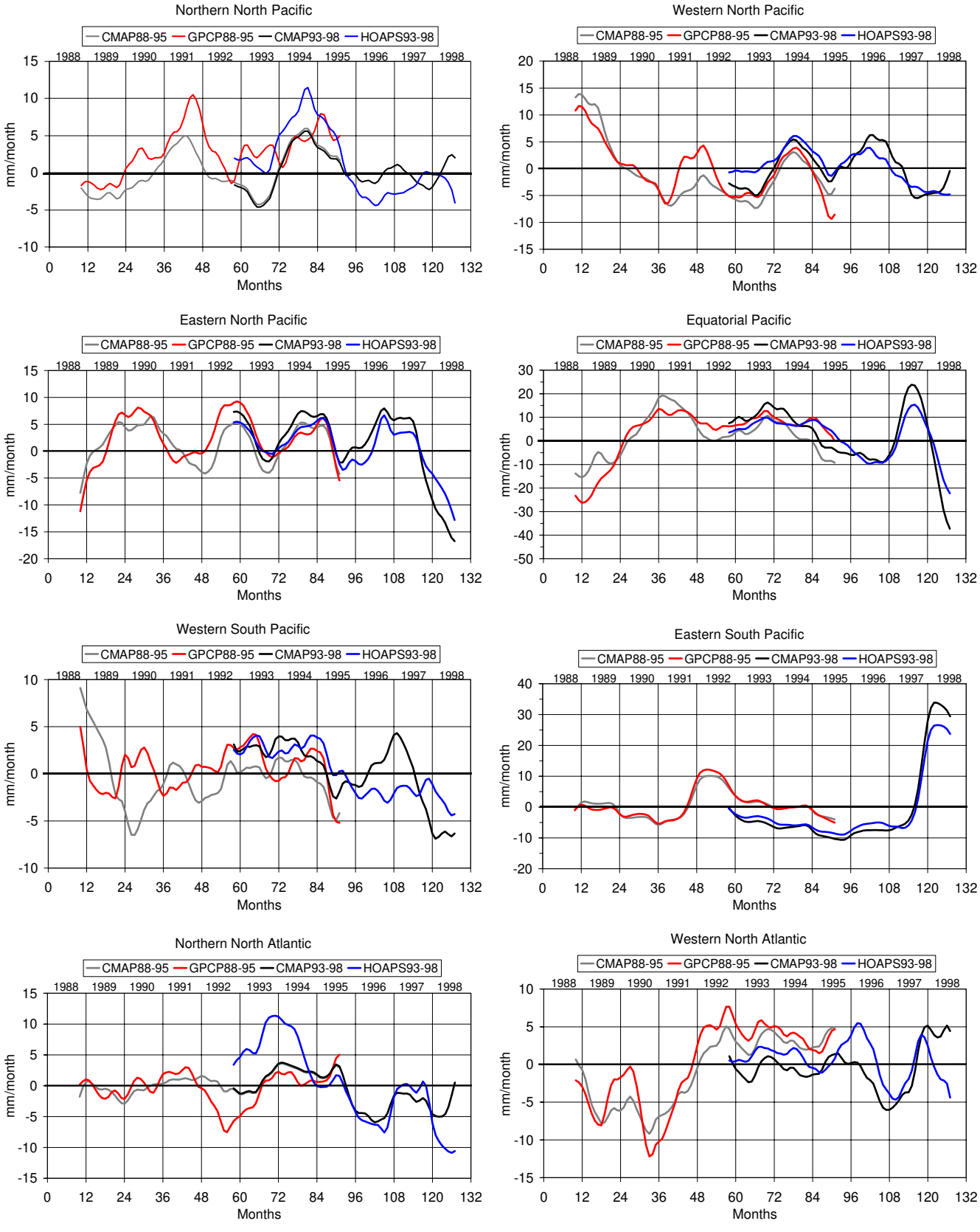

of the variations than on the phase, which generally shows a reasonable agreement. However, we could not find two data sets that agree over the whole period and for every region. Agreement rarely occurs for more than 3 years before an event occurs for which data sets disagree. Nevertheless, some consistent behaviour (for example related to El Nino events) was observed to be common to all data sets. It was also encouraging to find that HOAPS, CMAP and GPCP have a quite comparable interannual variability over their respective common periods, over most (but not all) ocean regions. Again, it was not possible to objectively discriminate the behaviour of the data sets with respect to their source. In general, the Indian Ocean and the Southern Ocean are regions where any consistency between data sets is hard to find, even between data sets of the same source.

It also happened that a specific data set has a behaviour in high disagreement with all the others. It is the case of MSU, which has a very peculiar seasonal cycle, and it is likely biased towards high (low) *P* in the first (second) part of the year in several ocean regions. We noticed that several geographical patterns, well-defined in most data sets, were not represented in in situ (COADS-derived) data sets. This is probably due to a problem in the method of interpolation or a drastic lack of observations. Concerning NWP re-analyses, NCEP shows, in general, a seasonal cycle of small amplitude. On the contrary, ECMWF produces the highest *P* values almost everywhere (and especially in the ITCZ and SPCZ), and has, by far, the largest interannual variations. Several general comments about satellite data are worthy of mention. Compared to the other data sets, they show less *P* in regions of low *P* like the eastern part of the subtropical gyres. However, they may be more correct there, in particular MSU, which is insensitive to non-precipitating cirrus clouds. Also, TOPEX and HOAPS, but to a lesser degree, show lower *P* than others in regions of high *P*. MSU does not follow, because it shows reasonably high values in regions of high *P*. An interesting point is that satellites may capture fine patterns such as the occurrence of the split of the ITCZ in March 1993 or the cut of the SPCZ, which are not present in COADS and not well-reproduced by NWP models, although they assimilate satellite data. Moreover, HOAPS data allows capturing additional *P* patterns due to its highest resolution compared to other data sets.

Composite data (GPCP and CMAP), which combine observations from several satellite and from rain gauges or NWP models, may represent the best recent data set available, despite a possible mean bias in regions of high *P* (CMAP clearly has the highest *P* in western tropics and in the equatorial band). However, these data sets never appear to be really "off" when compared to other data sets over the selected ocean regions, and they appear as the most coherent data sets in terms of seasonal and interannual variability over the period they cover, although this is only quantified by the large correlation coefficient (above 0.8) found between the low-frequency time series. For these reasons, and also because it covers a remarkably long period (20 years), the CMAP product would be our present choice to drive an OGCM. It is also used by Large and Yeager (2004) for the definition of the freshwater component of the diurnal to decadal global forcing for ocean and sea ice models they designed for Coordinated Ocean Reference Experiments.

The agreement noticed between GPCP, CMAP and HOAPS is also quite encouraging, as it suggests that some convergence is occurring despite supposed differences in data source and processing. Nevertheless, satellites do not cover the global ocean and there are still uncertainties linked to empirical algorithms.

Thus, progress in knowledge needs to be continued. Long time series are needed and then reanalysis efforts have to be periodically repeated at NWP. The *P* fields from the most recent NCEP2 and ERA40 re-analyses should be soon included in a similar evaluation study; methods to combine satellite, in situ and model data still have to be developed or improved.

Acknowledgements Authors are supported by CNRS (Centre National de la Recherche Scientifique), MESR (Ministère de l'Enseignement Supérieur et de la Recherche) and RAS (Russian Academy of Science). This work is a contribution to the Clipper project, which got support from INSU (Institut National des Sciences de l'Univers), Ifremer, CNES (Centre National d'Etude Spatiale), SHOM (Service Hydrographique de la Marine), and Météo-France. ECMWF analyses were made available by the AVISO vent-flux database in Toulouse. Finally, we would like to thank colleagues who kindly made their data sets available from the Web.

References

Adler RF, Kidd C, Petty G, Morissey M, Goodman HM (2001) Intercomparison of global precipitation products: the third precipitation intercomparison project (PIP-3). Bull Am Meteorol Soc 82(7):1377–1396

Ballabrera-Poy J, Murtugudde R, Busalacchi AJ (2002) On the potential impact of sea surface salinity observations on ENSO predictions. J Geophys Res 107(c12) 8007. DOI 10.1029/2001JC000834

Barnier B (1998) Forcing the ocean. In: Chassignet and Verron (eds) Ocean modeling and parameterization, vol 516. Kluwer, Netherlands, pp 45–80

Bauer P, Schluessel P (1993) Rainfall, total water, ice water, and water vapour over sea from polarised microwave simulations and special sensor microwave/imager data. J Geophys Res 98:20737–20759. (http://www.hoaps.zmaw.de)

Baumgartner A, Reichel E (eds) (1975) The world water balance. Elsevier, New York, p 179

Béranger K, Siefridt L, Barnier B, Garnier E, Roquet H (1999) Evaluation of operational ECMWF surface freshwater fluxes over oceans during 1991–97. J Mar Syst 22:13–36

Carmillet V, Brankart J-M, Brasseur P, Drange H, Evensen G, Verron J (2001) A singular evolutive extended Kalman filter to assimilate ocean colour data in a coupled physical–biochemical model of the North Atlantic Ocean. Ocean Model 3:167–192

Chen G, Chapron B, Tournadre J, Katsaros K, Vandemark D (1997) Global oceanic precipitation: A joint view by TOPEX and the TOPEX microwave radiometer. J Geophys Res 102:10457–10471

Da Silva A, White G (1996) Intercomparison of surface marines fluxes from the GEOS-1/DAS and NCEP/NCAR reanalyses. In: WCRP workshop on air–sea flux fields for forcing ocean models and validating CGMS, ECMWF, Reading, UK, 24–27 October 1995 (WMO/TD-N. 762)

Da Silva A, Young C, Levitus S (1994) Atlas of surface marine data 1994. In: Anomalies of fresh water fluxes, NOAA Atlas NESDIS 9, vol 4. U.S. Department of Commerce, NOAA, NESDIS. (http://www.nodc.noaa.gov)

Delcroix T, Henin C, Porte V, Arkin P (1996) Precipitation and sea surface salinity in the tropical Pacific Ocean. Deep-Sea Res Part 1 43(C7):1123–1141

Dorman CE, Bourke RH (1978) A temperature correction for Tucker's ocean rainfall estimates. Q J R Meteorol Soc 104:765–773

Erbert EE, Manton MJ, Arkin PA, Allam RJ, Holpin GE, Gruber A (1996) Results from the GPCP algorithm intercomparison program. Bull Am Meteorol Soc 77(12):2275–2887

Font J, Lagerloef G, LeVine D, Camps A, Zanife OZ (2004) The determination of surface salinity with the European SMOS space mission. IEEE T Geosci Remote 42(10):2196–2205

Ferry N, Reverdin G (2004) Sea surface salinity interannual variability in the western tropical Atlantic: an ocean general circulation model study. J Geophys Res 109(C05026). DOI 10.1029/2003JC002122

Garnier E, Barnier B, Siefridt L, Béranger K (2000) Investigating the 15 years air–sea flux climatology from the ECMWF re-analysis project as a surface boundary condition for ocean models. Int J Climatol 20(14):1653–1673

Gibson JK, Kallberg P, Uppala S, Hernandez A, Nomura A, Serrano E (1997) ECMWF re-analysis project report series, ECMWF Report

Glecker PJ, Weare BC (1997) Uncertainties in global surface heat flux climatologies derived from ship observations. J Clim 10:2764–2781

Grassl H, Jost V, Kumar R, Schulz J, Bauer P, Schluessel P (2000) The Hamburg ocean–atmosphere parameters and fluxes from satellite data (HOAPS): a climatological atlas of satellite-derived air–sea-interaction parameters over the oceans Report No. 312, ISSN 0937-1060. Max Planck Institute for Meteorology, Hamburg

Gruber A, Su X, Kanamitsu M, Schemm J (1999) The comparison of two merged rain gauge satellite precipitation datasets. Bull Am Meteorol Soc 81(11):2631–2644

Huffman GJ, Adler RF, Arkin P, Chang A, Ferraro R, Gruber A, Janowiak J, McNab A, Rudolf B, Schneider U (1997) The global precipitation climatology project (GPCP) combined precipitation data set. Bull Am Meteorol Soc 78(1):5–20

Josey SA, Kent EC, Taylor PK (1999) New insights into the ocean heat budget closure problem from analysis of the SOC air sea flux climatologies. J Clim 12:2856–2880. (http://www.soc.soton.ac.uk/JRD/MET/fluxclimatology.html)

Kalnay E, Kanamistu M, Kistler R, Collins W, Deaven D, Gandin L, Iredell M, Saha S, White G, Woolen J, Zhu Y, Cheliah M, Ebisuzaki W, Higgins W, Janowiak J, Mo CK, Ropelewski C, Leetma A, Reynolds R, Jenne R (1996) The NCEP/NCAR reanalysis project. Bull Am Meteorol Soc 77:437–471. (http://www.cisl.ucar.edu/)

Kidds C (2001) Satellite rainfall climatology: a review. Int J Climatol 21(9):1041–1066

Killworth PD, Smeed DA, Nurser AJG (2000) The effects on ocean models of relaxation toward observations at the surface. J Phys Oceanogr 30(1):160–174

Large W, Yeager S (2004) Diurnal to decadal global forcing for ocean and sea ice models: the data sets and flux climatologies. NCAR technical note: NCAR/TN-460+STR. CGD Division of the National Center for Atmospheric Research, Boulder, Colorado

Large WG, Danabasoglu G, Doney SC (1997) Sensitivity to surface forcing and boundary layer mixing in a global ocean model: annual mean climatology. J Phys Oceanogr 27:2418–2447

Legates D, Willmott C (1990) Mean seasonal and spatial variability in gauge-corrected global precipitation. Int J Climatol 10:111–127

Marchesiello P, McWilliams JC, Shchepetkin A (2003) Equilibrium structure and dynamics of the California Current System. J Phys Oceanogr 33:753–783

Quartly GD, Srokosz MA, Guymer TH (1999) Global precipitation statistics from dual-frequency TOPEX altimetry. J Geophys Res 104:31489–31516. (anonymous ftp://ftp.soc.soton.ac.uk, cd pub/TOPEX_GPS)

Rudolf B, Hauschild H, Ruth W, Schneider U (1996) Comparison of rain gauge analysis, satellite-based precipitation estimates, and forecast model results. Ad Space Res 18:53–62

Schmitt RW (1995) The ocean component of the global water cycle. (US national report to International Union of Geodesy and Geophysics 1991–94). Rev Geophys 33(Supplement, Pt. 2): 1395–1409

Siefridt L, Barnier B, Béranger K, Roquet H (1999) Evaluation of ECMWF surface heat fluxes as a thermal ocean forcing in relation to model parameterisation changes during the period 1986 to 1995. J Mar Syst 19:113–135

Smith RD, Maltrud ME, Bryan FO, Hecht MW (2000) Numerical simulation of the North Atlantic Ocean at 1/10°. J Phys Oceanogr 30:1532–1561

Speer K, Tziperman E (1992) Rates of water mass formation in the North Atlantic Ocean. J Phys Oceanogr 22:93–104

Spencer RW (1993) Global oceanic precipitation from the MSU during 1979–91 and comparisons to other climatologies. J Clim 6:1301–1326. (http://ingrid.ldeo.columbia.edu/SOURCES/.NASA/.msu)

Tiedtke M (1993) Representation of clouds in large-scale models. Mon Weather Rev 121:3040–3061

Tréguier AM, Boebel O, Barnier B, Madec G (2003) Agulhas eddy fluxes in a 1/6° Atlantic model. Deep-Sea Res Part 2 50:251–280

Tucker GB (1961) Precipitation over the North Atlantic Ocean. Quart J Roy Meteor Soc 87:147–158

von Storch H, Zwiers FW (1999) Statistical analysis in climate research. Cambridge Univ. Press, Cambridge, UK, pp 503

WCRP-115 (2001) World Climate Research Programme/Scientific Committee on Oceanic Research (WCRP/SCOR) Workshop on Intercomparison and validation of ocean–atmosphere flux fields, Bolger Center, Potomac, MD, USA, 21–24 May 2001. In: White G (ed) WMO-TD-N° 1083

White GH (1995) An intercomparison of precipitation and surface fluxes from operational NWP analysis/forecast systems, Report N°22, WMO/TD-N723

Willebrand J, Barnier B, Claus BN, Dieterich C, Killworth PD, Le Provost C, Yanli Jia J-M, Molines J-M, New AL (2001) Circulation characteristics in three eddy-permitting models of the North Atlantic. Prog Oceanogr 8(2–3):123–161

Woodruff SD, Slutz RJ, Jenne RL, Steurer PM (1987) A comprehensive ocean atmosphere data set. Bull Am Meteorol Soc 68:1239–1250

Xie P, Arkin PA (1997) Global precipitation: a 17-year monthly analysis based on gauge observations, satellite estimates, and numerical model outputs. Bull Am Meteorol Soc 78(11):2539–2558. (anonymous ftp://ftp.ncep.noaa.gov, cd pub/precip/cmap/monthly)